
Post-Generation Curation of Synthetic Images via Homogeneous-Heterogeneous Splitting

Disheng Liu Tuo Liang Chaoda Song Yu Yin*
Department of Computer and Data Sciences
Case Western Reserve University
Cleveland, OH, USA
{dx1952, tx1859, cxs965, yxy1421}@case.edu

Abstract

Recent generative models can produce high-quality synthetic images, offering scalable training data for data-hungry models. Existing approaches to exploiting this potential typically involve 1) training or fine-tuning generators, or 2) using lightweight post-hoc adaptation like prompt engineering or inference-time guidance, making them generator-specific and expertise-intensive. We study a complementary question: *given a fixed pool of generated images, can downstream utility be improved purely by selecting an informative subset?* The answer is yes. We show that effective selection must counter a structural bias of modern generators: they tend to over-produce canonical modes of each class while under-representing intra-class variation. Building on this insight, we split each real class into a *canonical Homogeneous (HO) subset* and a *non-redundant Heterogeneous (HE) subset*, then score synthetic images by a fidelity-diversity criterion that rewards semantic alignment while penalizing canonical redundancy. The method is generator-agnostic and requires no retraining. Across multiple benchmarks, it consistently outperforms state-of-the-art data selection baselines and matches the real-data performance with up to 40% fewer synthetic samples. The same criterion remains effective when applied on top of stronger task-tuned generators, with gains on both classification and segmentation tasks. Post-generation selection is therefore not a substitute for better generators, but a complementary mechanism for improving the utility of synthetic data.

1 Introduction

Generative models (GMs) produce high-quality synthetic data and offer a promising solution for data scarcity in data-intensive AI. Recent studies demonstrate that GMs can effectively replicate datasets (*e.g.*, CIFAR-10, ImageNet) and improve downstream models trained on such synthetic data in generalization, transferability, and in-domain accuracy [1–6].

However, practical challenges remain: 1) synthetic datasets may contain low-fidelity or mislabeled samples, introducing harmful noise; 2) Inadvertently over-representing dominant patterns could transfer inherent biases to downstream models; 3) While scaling the data alleviates these issues, it incurs higher computational overhead and longer training times.

To harness synthetic data, researchers are prioritizing improved generation techniques that yield more faithful and diverse data. These approaches can be broadly categorized into: 1) training- or fine-tuning-based methods [3, 7], which adapt generators to better match target distributions; 2) lightweight strategies like guidance [8–12] or prompting [13–15]. While effective, these approaches face distinct

*Corresponding author.

trade-offs: training-based methods incur substantial computational overhead due to the optimization of large-scale models, whereas lightweight strategies often rely on model-specific configurations, significant domain expertise, or extensive empirical tuning. Alternatively, data selection [16, 17] separates quality control from the image generation, bypassing the typical pitfalls of steering-based methods. This data-centric focus serves as a practical and complementary refinement stage, ensuring high-quality synthetic outputs even after specialized, task-guided generation phases.

Aligning curated data with the target distribution is a promising post-processing principle. Image-Label Alignment methods [4, 18, 19] assume that high-quality data align strictly with the generative labels, employing pre-trained discriminators to filter out noisy samples; Image-Image Alignment [20, 21] prioritizes synthetic samples that closely resemble real images. Both strategies emphasize fidelity, but largely neglect diversity, reducing the utility of synthetic data [6] due to repeated patterns and missing novel information.

Motivated by these limitations, we propose a *fidelity-diversity* balanced post-generation curation framework to enhance the utility of synthetic imagery for downstream tasks. In the curation pipeline, we first split the real dataset into two subsets: a **Homogeneous** set characterized by high internal similarity, and a **Heterogeneous** set enriched with variation. Based on this partitioning, we design a scoring mechanism to identify and select desired synthetic instances, balancing high semantic quality with representational diversity, shown as Fig. 1). Concretely, we compute two complementary metrics: 1) *fidelity scores*, measuring semantic similarity to real samples; 2) *diversity scores*, quantifying the deviation from repetitive patterns. Combining such metrics, we curated the final desired synthetic pool.

To quantify the utility of our curation strategy, experiments are implemented across diverse datasets (e.g., CIFAR-10, ImageNet, etc.) and architectures (e.g., ResNet, ViT). We synthesize data pools using generators trained on target distributions, then apply the curation method to train downstream models for in- and out-of-distribution testings. Furthermore, we apply the curation as a post-process after optimized generations for downstream tasks. Empirical results demonstrate the validity of our post-generation processing under the different settings. In summary, our contributions are as follows:

1. A nearest-neighbor-cover partition (HO-HE) of real data with a minimality guarantee (Prop. 1), giving an explicit notion of canonical vs. non-redundant samples.
2. A principled, post-generation selection strategy that jointly quantifies and balances fidelity and diversity. The framework is generator-agnostic, requiring only a synthetic data pool, and avoids costly retraining or fine-tuning of generators.
3. Extensive experiments validate the approach across classification and segmentation benchmarks with multiple generators and backbones. Our method consistently improves in-domain accuracy and OOD robustness over baselines, plus an additional plug-in evaluation on top of generator-side intervention methods.

2 Related Works

2.1 Curating Synthetic Data for downstream utility

Synthetic data has emerged as a promising solution to data scarcity in the AI era [22–24]. Recent studies show that models trained on synthetic data can learn robust visual representations [4, 25–28]. Moreover, augmenting real datasets with synthetic samples has been shown to further improve model performance [2, 29, 30]. However, the distribution gap between real and synthetic data [6, 31] highlights the need for careful tailoring [5, 24, 32, 33] to fully exploit the potential of synthetic data.

Intervening before or during generation is an effective way to improve the utility of synthetic data. Fine-tuning-based methods adapt generators to target distributions or downstream tasks [3, 7], while prompt-, guidance-, and sampling-based methods steer generated samples toward desired classes,

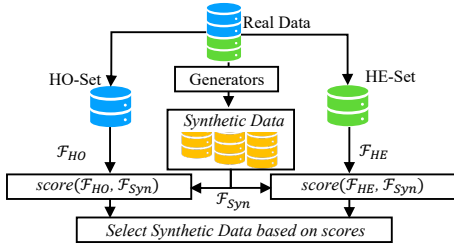


Figure 1: Data selection while considering both fidelity and diversity. Real data (targeted distribution) is divided into the HO-Set and the HE-Set. Synthetic instances are then scored by referring to these two partitions for subsequent selection.

attributes, or harder variations [8–10, 14]. Although these approaches can improve the utility of synthetic data, they often require generator access, task-specific tuning, prompt expertise, or additional generation cost. In contrast, post-generation curation offers a practical and scalable alternative to generation-time intervention for improving synthetic data utility.

2.2 Post-Generation Synthetic Data Curations

Unlike real data pruning [17, 34, 35], synthetic data usage involves generator bias, distribution drift, and mode collapse. Such artifacts require careful curation to steer synthetic pool toward the target.

Fidelity-Guided Curation. High-fidelity generations ensure semantic correctness, making fidelity-based selection effective. Such curation strategies can be broadly categorized into two main approaches: **1) Image-Label Alignment:** pretrained or task-specific models are used to filter low-quality samples by discarding those misclassified within top- k predictions [36–39]. Concretely, CLIP [40] is used to assess image-label semantic alignment [4, 21, 41]; **2) Image-Image Alignment:** this approach quantifies similarity between synthetic and real images to filter out low-quality data that deviate from the real distribution [20, 21, 42, 43]. Specifically, clustering-based curation [21] use real-data cluster centroids as anchors to retrieve synthetic samples. While straightforward, these methods rely heavily on visual similarity and risk reducing data diversity for downstream tasks.

Diversity-Guided Curations. As generative images become increasingly realistic, diversity is key for downstream usage. Prior works enhance diversity by varying prompts [13], applying text-conditioned augmentation [15, 44], using textual inversion [45], or conditioning on classifier outputs [46]. While effective, these methods require fine-tuning or prompt engineering and focus on generation-time diversity, offering little guidance on how to efficiently leverage existing synthetic datasets. Building the priors, we curate synthetic datasets by jointly considering fidelity and diversity, without modifying generative model output, forming a post-generation data curation pipeline.

3 Methods

Overview. We target the following *post-generation curation* problem and assume only sample access to the generator. Given (i) a labeled real reference set $\mathcal{D}_R = \{(I_i, y_i)\}_{i=1}^{|\mathcal{D}_R|}$, (ii) a synthetic pool $\mathcal{D}_S = \{\tilde{I}_j\}_{j=1}^{|\mathcal{D}_S|}$ with class assignments inherited from the generator’s conditioning, and (iii) a selection budget k (possibly much larger than $|\mathcal{D}_R|$), the goal is to select $\mathcal{A} \subseteq \mathcal{D}_S$ so that the selected synthetic training set improves downstream classification on the real distribution.

Our method has two steps. First, we split the real reference images into a *Homogeneous* subset \mathcal{I}_{HO} of local representatives and a *Heterogeneous* subset \mathcal{I}_{HE} of non-redundant variation (Sec. 3.1). Second, we allocate the synthetic budget across these two subsets and score each synthetic candidate with a partition-conditioned fidelity–diversity criterion (Sec. 3.2). The key design principle is that the selected set should match both the canonical component and the heterogeneous component of the real class, instead of ranking all synthetic images against a single pooled reference distribution.

3.1 Categorizing Homogeneous (HO) and Heterogeneous (HE) Samples

To guide the selection of synthetic data, we first categorize target real distribution into two distinct sets: **Homogeneous (HO)** and **Heterogeneous (HE)**. HO instances represent the canonical semantics, exhibiting high intra-class similarity in feature space. HE instances capture greater variation, including less typical instances that contribute to diversity.

Identifying HO and HE Instances. We construct the HO/HE split from the directed 1-nearest-neighbor (1-NN) graph of each real class in feature space. The construction is local, non-parametric, and costs $O(n^2d)$ for a class with n examples and d is the feature dimension of input. Unlike a centroid-near/far split (e.g., k -means, core-set partitions), it does not impose a global axis through the class: \mathcal{I}_{HO} contains examples that other examples use as their closest local representatives, while \mathcal{I}_{HE} contains examples with zero in-degree in this local graph.

Given images $\mathcal{I} = \{I_1, \dots, I_n\}$, we extracted ℓ_2 -normalized features $\mathcal{F} = \{f_1, \dots, f_n\}$ using a pretrained encoder (e.g., MoCo v3 [47]). We use cosine distance $d(f_i, f_j) = 1 - \langle f_i, f_j \rangle$ throughout.

For each I_i , we define its within-class nearest neighbor

$$j^*(i) = \arg \max_{j \neq i} \langle f_i, f_j \rangle. \quad (1)$$

Therefore, the HO set is the image of this map and the HE set is its complement:

$$\mathcal{I}_{HO} = \{I_i : \exists j \neq i, j^*(j) = i\}, \quad \mathcal{I}_{HE} = \mathcal{I} \setminus \mathcal{I}_{HO}. \quad (2)$$

Equivalently, in the directed 1-NN graph with edges $I_i \rightarrow I_{j^*(i)}$, \mathcal{I}_{HO} is the set of nodes with positive in-degree and \mathcal{I}_{HE} is the set of zero in-degree nodes.

Proposition 1 (\mathcal{I}_{HO} as a minimal nearest-neighbor cover). *Assume every sample has a unique within-class nearest neighbor. Then \mathcal{I}_{HO} is the unique inclusion-minimal subset $A \subseteq \mathcal{I}$ such that*

$$\min_{I_i \in A, i \neq j} d(f_j, f_i) = \min_{I_i \in \mathcal{I}, i \neq j} d(f_j, f_i), \quad \forall I_j \in \mathcal{I}. \quad (3)$$

Thus, with $\varepsilon = \max_j d(f_j, f_{j^*(j)})$, every real sample has an \mathcal{I}_{HO} representative within distance ε .

Proposition 1 formalizes the representative role of \mathcal{I}_{HO} : replacing the full class by \mathcal{I}_{HO} preserves the nearest-neighbor reconstruction cost of every training image. The complement \mathcal{I}_{HE} should therefore not be read as noise or outliers. It is the part of the class that is not needed as a nearest-neighbor representative for other examples, and is precisely where non-redundant variation can be lost when a generator over-produces canonical images.

Empirical $\mathcal{I}_{HO} - \mathcal{I}_{HE}$ Analysis and Impact. As visualized in Fig. 2, the HO-HE split preserves local neighborhood and keeps each semantic mode mixed across both subsets, avoiding mode imbalance during guided selection. In contrast, centroid-based alternatives that define near/far canonical patterns tend to isolate individual mode regions, yielding suboptimal selection references. Without a complete semantic landscape, prioritizing any single mode during synthetic data curation inevitably overlooks parts of the real distribution, leading to information loss. We also show HO-HE partition instances in CIFAR-10 (Fig. 3). Because HO samples are retrieved as local representatives, they have higher intra-class similarity than HE samples, both visually and quantitatively (more cases in Appendix Fig. 10 and Tab. 7).

Although both \mathcal{I}_{HO} and \mathcal{I}_{HE} encompass all distribution modes, we observe an interesting divergence in downstream behaviors: 1) **GMs preferentially learn and reproduce \mathcal{I}_{HO} .** As quantified in Fig. 4, synthetic data disproportionately mirrors \mathcal{I}_{HO} over \mathcal{I}_{HE} . This inherent preference indicates that GMs gravitate toward repeated canonical patterns within \mathcal{I}_{HO} , which may explain the persistent diversity limitations observed in modern generative models. 2) **Discriminators exhibit a similar performance bias, excelling on \mathcal{I}_{HO} while struggling with \mathcal{I}_{HE} .** This discrepancy indicates that, despite sharing underlying semantics, \mathcal{I}_{HE} contains inherently more challenging cases that discriminators fail to model effectively (empirical supports across datasets is provided in the Appendix C, Fig. 13).

3.2 Synthetic Data Selection Strategy

Given the HO and HE sets, we propose a synthetic data selection strategy to identify desirable instances from a fixed synthetic pool. The core objective is to ensure high semantic fidelity while enhancing diversity by prioritizing samples that diverge from the dominant patterns in HO.

Partitioned Selection Strategy. Unlike prior methods that treat the entire real dataset as a single reference for data selection, we propose a partitioned selection approach. We treat HO and HE as separate partitions and select synthetic instances by referring to real images within each partition under the same principle: desired synthetics should be sufficiently close to their corresponding real instances, while prioritizing those that deviate from canonical representations. By combining the selection results from HO and HE instances, we obtain the final selected pool.

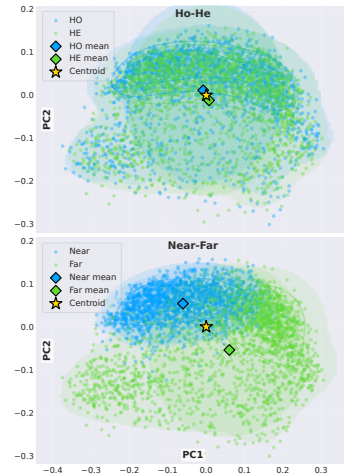


Figure 2: PCA of the CIFAR-10 “horse” class under different partitioning rules. The 1-NN *HO-HE split (top)* preserves local neighborhood, whereas *centroid-based split (bottom)* cuts a class along a single global axis.

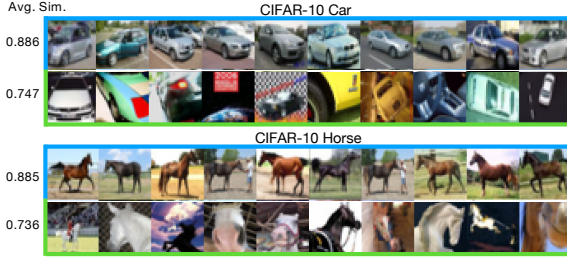


Figure 3: HO and HE instances in CIFAR-10. *Avg. Sim.* represents the average similarity between the images in each row and the entire class. HO instances are more representative, expressing the core semantics. HE instances are more diverse, capturing a broader range of variations (More examples are in the Appendix Fig.10).

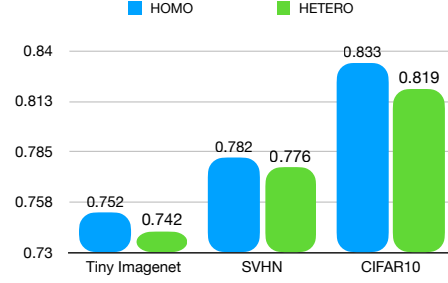


Figure 4: Similarity between the synthetic and HO, HE splits. We measure cosine similarity between HO/HE subsets and generations of models trained by each real dataset. Synthetic data consistently more closely resembles HO than HE.

Concretely, we compute a selection score S^p for each synthetic sample based on its correlation with partition $p \in \{\text{HO}, \text{HE}\}$. Samples are ranked within each partition, and the instances with high S^p get retrieved. Alg. 1 for the pseudo-code of our selection procedure.

Scoring Mechanism for Each Partition.

Our selection mechanism balances two competing objectives: the *fidelity score*, measuring how closely a synthetic instance resembles the real, and the *diversity score*, measuring how much it deviates from canonical patterns in the real dataset.

1) *Fidelity Score*. The fidelity score S_{fid}^p quantifies how well the synthetic samples align with the real distribution of partition p . We measure this using the cosine similarity between the synthetic features \mathcal{F}^{syn} and the real features \mathcal{F}^p , as defined in Eq. 4. A higher fidelity score indicates that the synthetic samples closely resemble the real data in the corresponding partition:

$$S_{\text{fid}}^p = \cos(\mathcal{F}^{\text{syn}}, \mathcal{F}^p). \quad (4)$$

2) *Diversity Score*. The diversity score S_{div}^p is designed to encourage the selected synthetic samples to deviate from canonical patterns. To achieve this, we define a subset-specific reference anchor \mathcal{R}^p . For the HO subset, the anchor is the centroid of the real features ($\mathcal{R}^{\text{HO}} = \mathcal{C}^{\text{HO}}$). For the HE subset, the anchor is the nearest matching feature in the HO subset ($\mathcal{R}^{\text{HE}} = \mathcal{F}^{\text{HO}}[\text{idx}]$). The diversity metric is then formulated as the negative cosine similarity between two directional vectors, as defined in Eq. 5: one from the real instance \mathcal{F}^p to the anchor \mathcal{R}^p , and the other from the same real instance to the synthetic data \mathcal{F}^{syn} (representative visual cases are shown in Fig. 14 of the Appendix).

$$S_{\text{div}}^p = -\cos(\mathcal{R}^p - \mathcal{F}^p, \mathcal{F}^{\text{syn}} - \mathcal{F}^p). \quad (5)$$

As illustrated in Fig. 5, if these two vectors point in opposite directions, the cosine similarity is negative, leading to a higher diversity score. If the vectors are aligned, the synthetic sample is closer to the homogeneous distribution, resulting in a lower diversity score.

Algorithm 1: Data Selection with HO and HE

Input: Feat. maps $\mathcal{F}^{\text{HO}} \in \mathbb{R}^{n \times d}$, $\mathcal{F}^{\text{HE}} \in \mathbb{R}^{m \times d}$, $\mathcal{F}^{\text{syn}} \in \mathbb{R}^{s \times d}$; centroid $\mathcal{C}^{\text{HO}} \in \mathbb{R}^d$; weight $\alpha \in [0, 1]$; size k

Output: Selected indices $\mathcal{I}_{\text{selected}}$

- 1: {Step 1: Construct reference anchors}
- 2: $\mathcal{R}^{\text{HO}} \leftarrow \mathcal{C}^{\text{HO}}$
- 3: $\text{idx} \leftarrow \text{argmax}(\mathcal{F}^{\text{HE}}(\mathcal{F}^{\text{HO}})^\top, \text{dim} = 1)$
- 4: $\mathcal{R}^{\text{HE}} \leftarrow \mathcal{F}^{\text{HE}}[\text{idx}]$ {Align HE features to HO}
- 5: {Step 2: Score calculation and selection}
- 6: **for** $p \in \{\text{HO}, \text{HE}\}$ **do**
- 7: $S_{\text{fid}}^p \leftarrow \cos(\mathcal{F}^{\text{syn}}, \mathcal{F}^p)$ {Fidelity}
- 8: $S_{\text{div}}^p \leftarrow -\cos(\mathcal{R}^p - \mathcal{F}^p, \mathcal{F}^{\text{syn}} - \mathcal{F}^p)$ {Diversity}
- 9: $S^p \leftarrow \alpha S_{\text{div}}^p + (1 - \alpha) S_{\text{fid}}^p$
- 10: $\mathcal{I}_{\text{top}}^p \leftarrow \text{Top}_k(S^p)$
- 11: **end for**
- 12: **return** Selected set $\mathcal{A} \leftarrow \mathcal{I}_{\text{top}}^{\text{HO}} \cup \mathcal{I}_{\text{top}}^{\text{HE}}$

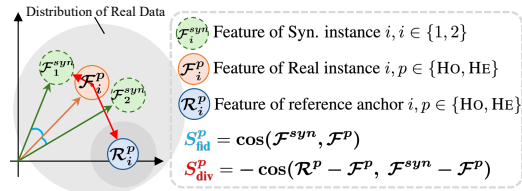


Figure 5: Illustration of the computation of S_{fid}^p and S_{div}^p in partition p . Fidelity is assessed as $\cos(\mathcal{F}_i^{\text{syn}}, \mathcal{F}_i^p)$, while diversity is measured by the angle between vectors ending at $\mathcal{F}_i^{\text{syn}}$ and \mathcal{R}_i^p . In the diagram, Syn. instance 1 exhibits greater diversity than Syn. instance 2.

3) *Total Score*. To control the trade-off between fidelity and diversity, we define the score as:

$$S^p = \alpha \cdot S_{\text{div}}^p + (1 - \alpha) \cdot S_{\text{fid}}^p, \tag{6}$$

where α is a hyperparameter that determines the selection priority. $\alpha = 0$ (*MaxSim*) prioritizes fidelity, ensuring that synthetic instances closely resemble real ones. $\alpha = 1$ (*MaxDiv*) prioritizes diversity, encouraging synthetic samples that deviate from the dominant patterns of real data. Adjusting α enables flexible control over the selection behavior to match downstream needs.

Practical Considerations. (a) **Complexity.** Building the 1-NN graph costs $O(n^2d)$ after feature extraction, where n is number of real samples, d is feature dimension. Scoring is implemented as batched matrix multiplication and costs $O(|\mathcal{D}_S|nd)$, where $|\mathcal{D}_S|$ denotes the number of synthetic candidates. (b) **Encoder choice.** The split is relative to encoder ϕ , so a domain-mismatched encoder can degrade curation. Sec. 5 compares representative encoders and shows that the gains are not tied to a single feature extractor. (c) **No balanced HO-HE requirement.** The HO-HE split is induced by the 1-NN graph; it does not assume a target ratio or require pre-labeled canonical examples. Unequal partition sizes only change how the synthetic budget is allocated across the two scoring branches: larger partitions receive proportionally more selections, while smaller partitions still receive explicit coverage. Thus, the near-balanced HO-HE masses observed in the experiments are an empirical property of the datasets, not a requirement of the method.

4 Experiments

We evaluate post-generation curation under two settings. The *general* setting fixes a generator and a synthetic pool, applies each selection method under the same budget, and trains downstream classifiers for in-domain (Sec. 4.2) and out-of-domain (OOD) (Sec. 4.3) evaluation. The *plug-in* setting (Sec. 4.4) applies the same curation step after task-customized generation to test whether selection remains useful when the generator has already been adapted to a downstream task.

4.1 Datasets and Baselines

Datasets. The main evaluation spans classification and segmentation datasets with increasing scale and visual complexity. For SVHN [48], CIFAR-10 [49], and Tiny-ImageNet [50], covering 10, 10, and 200 classes respectively, we curate synthetic pools generated by EDM [51]. For large-scale validation, we use ImageNet-1K (IN-1K) synthetics generated by EDM2 [52, 53]. In total, the evaluation covers 4 in-domain benchmarks and 9 OOD benchmarks. The plug-in experiments further use task-customized generation for ImageNet-100 (IN-100) [54] and VOCaug [55] (Sec. 4.4).

Baselines. For each comparison, all selection methods operate on the same synthetic pool and use the same selection budget. In the main evaluation, we compare three categories of selection methods. *RandSelect* [56–58] is an uninformed random baseline. *CLIP-Align* [4] represents image-label alignment by ranking generated images with CLIP text-image scores. *RealScore* [20] and *SBSim* [21] represent image-image alignment. In the plug-in setting, the baselines are generation-side interventions that already target the downstream task: inference-time intervention [59] and the fine-tuned generator *JoDiffusion* [60].

Implementation. Unless otherwise stated, we use $\alpha = 0.5$ for all main experiments and keep the downstream training recipe fixed within each comparison.

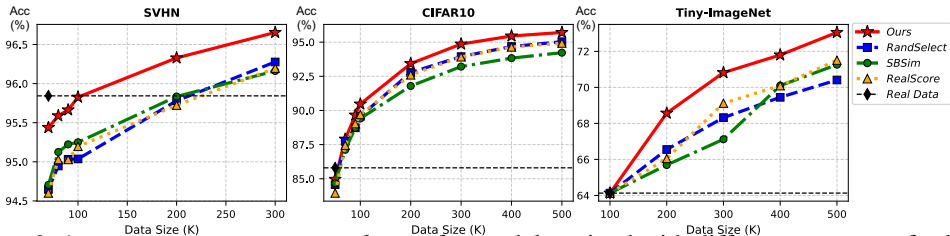


Figure 6: Average test accuracy over 6 runs for models trained with different amounts of selected synthetic data. We compare with *RandSelect*, *SBSim*, and *RealScore*; *CLIP-Align* is omitted for readability, with full results in Appendix Tabs. 10, 11, and 12. The black dashed line denotes the corresponding real-data baseline.

Table 1: ImageNet-1K Top-1 Acc. (%) with 1M and 3M selected samples. Background colors indicate different models: ViT-B/16 and ResNet-50, evaluated under both **from-scratch** and **fine-tuning** settings. The corresponding training recipes are provided in Appendix E.2.

Selection	Scratch						Fine-tune			
	+0	+1M	+3M	+0	+1M	+3M	1M	3M	1M	3M
Random	64.22	70.90	73.54	69.27	72.03	72.13	78.52	78.68	71.90	73.65
RealScore	-	70.92	73.53	-	72.01	72.16	78.52	78.67	71.93	73.62
CLIP-Align	-	69.18	70.88	-	69.44	70.98	72.40	75.23	62.57	67.57
SBSim ($\alpha = 0$)	-	70.95	73.23	-	71.97	72.18	78.58	78.76	72.18	74.14
Diversity ($\alpha = 1$)	-	71.42	73.79	-	71.80	73.25	78.72	79.14	72.25	74.25
Ours	-	71.49	74.02	-	72.09	73.33	78.97	79.36	73.14	74.76

4.2 Scaling Model Performance with Selective Synthetic Data

We first ask whether curation improves the value of synthetic data as the training budget grows. For each selected set, we train the same downstream architecture with the same recipe and evaluate on the corresponding real test set. The small- and medium-scale experiments use ResNet-18/50 [61] and EfficientNet-B0 [62]; the IN-1K experiments further include ViT-B/16 [63]. Full training details are provided in Appendix E.2.

Across **SVHN**, **CIFAR-10**, and **Tiny-ImageNet**, Fig. 6 shows consistent gains from our curation, with the largest benefits appearing as the selection budget grows. On **SVHN**, our method matches the real-data baseline with substantially fewer examples (*i.e.*, 100k synthetic samples), whereas alternative methods require over 200k to reach comparable accuracy. On **CIFAR-10**, our method achieves 95% accuracy with 300k samples, while *RandSelect* and *RealScore* require around 500k, and *SBSim* demands substantially more. This pattern is consistent with the failure mode targeted by our method: once high-fidelity canonical samples saturate, additional gains depend on selecting less redundant variation. For the harder **Tiny-ImageNet**, we use selected synthetic data as augmentation since synthetic-only training suffers a larger domain gap; our curation improves ResNet-50 accuracy at every augmentation budget.

For **IN-1K**, prior work [2, 3, 6] reported a persistent gap between real and synthetic data at ImageNet scale. We therefore evaluate two practical uses of selected synthetic data: 1) training models from scratch with synthetic data as augmentation and 2) fine-tuning pre-trained models using synthetic data alone. Tab. 1 reports results for ViT-B/16 and ResNet-50 with 1M and 3M selected images from an EDM2 pool. Using the same training configuration, our method gives the best accuracy across all settings, indicating that the fidelity–diversity balance remains useful at ImageNet scale.

4.3 Enhancing Model Generalizability with Selected Samples

Models trained on informative and diverse data are expected to achieve greater robustness under OOD settings. In this part, we evaluate the generalizability of the best models trained (from scratch) in the previous section with OOD datasets. The results demonstrate that curated synthetic data improves model generalizability.

OOD of Tiny-ImageNet. We use Tiny-ImageNet-C [64], which incorporates various types of corruption. We classify them into three types: color-variation set (*i.e.*, brightness adjustment, contrast variation), noise-variation set (*i.e.*, pixelation, Gaussian noise, motion blur), and compression-variation set (*i.e.*, JPEG compression). The results are reported in Fig. 7(a). **OOD of IN-1K.** We use several OOD datasets and categorize them into two groups 1) *original suite*, including ImageNet-V2 [65] and

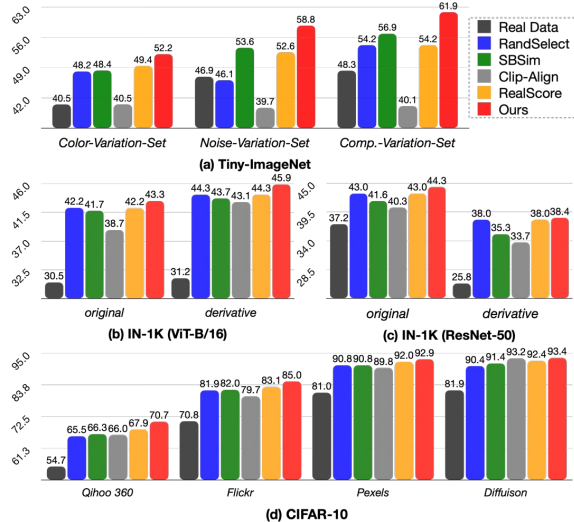


Figure 7: OOD Evaluation. Among different settings, ours consistently achieves the best performance.

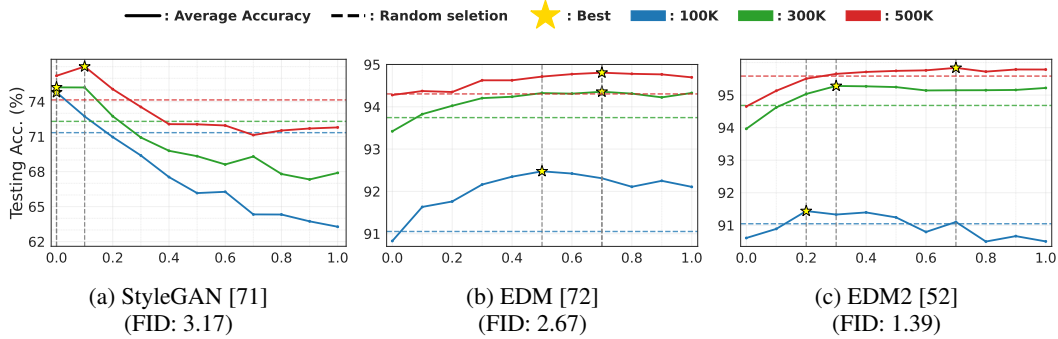


Figure 8: Testing accuracy versus trade-off α ($0 = \text{fidelity}$, $1 = \text{diversity}$). Each subfigure compares the 100K, 300K, and 500K settings with trend lines, and the optimal point on each curve is marked by a star. Results are reported with **ResNet-18** using the **average accuracy over 8 runs**.

ImageNet-Sketch [66]; 2) *derivative suite*, including ImageNet-C [67], -Drawing, and -Cartoon [68], derived from the validation set (Appendix E.4 for details). The evaluation results are summarized in Fig. 7(b), (c). **OOD of CIFAR-10**. CIFAR-10-Warehouse [69] is used as a benchmark, collecting data from diverse sources (*e.g.*, different search engines). The results are reported in Fig. 7(d). More results (*i.e.*, OOD of SVHN, examples of OOD data) are presented in Appendix E.4.

4.4 Plug-in Curation after Generator-Side Interventions

We next test whether curation remains useful after the synthetic pool has already been improved by a generator-side intervention. Keeping each task-adapted pool fixed, we apply our selection as a plug-in post-processing step. We study two representative intervention types: inference-time generator intervention for classification [59] and generator fine-tuning for segmentation [60].

Classification. We apply our curation to synthetic images generated with inference-time intervention [59] on IN-100, then train ResNet-18 on the selected data. As shown in Tab. 2, our curation further improves synthetic data utility: curation provides both an equal-budget gain and a 40–50% data reduction on task-aware samples.

Segmentation. We curate synthetic VOCAug data produced by the fine-tuned generator JoDiffusion [60], then train the downstream segmentation model (*i.e.*, DeepLabV3 [70]). In Tab. 3, we report mIoU, showing that our method provides additional gains on top of customized generation via fine-tuning. Overall, both results suggest that post-generation curation is a generator-agnostic approach that further improves the utility of optimized synthetic data, highlighting the practical value of our curation strategy.

Table 2: Our curation achieves comparable or better accuracy with fewer synthetic samples on IN-100 using ResNet-18.

Size ([59]→Ours)	Acc. ([59]→Ours)	Reduction
50k→30k	78.14→79.00	40%
100k→50k	79.36→79.48	50%

Table 3: Post-generation curation improves DeepLabV3+ performance in mIoU across synthetic data sizes.

Synthetic Size	JoDiffusion [60]	+ Ours
10k	73.61	74.94
15k	73.87	76.04

5 Analysis and Discussion

CLIP Filtering Biases Toward Canonical Modes. The weak performance of *CLIP-Align* in Sec. 4.2 suggests that image–text alignment alone is not a sufficient selection criterion. Tab. 4 provides a quantitative diagnostic on CIFAR-10: High-CLIP-score samples are consistently closer to \mathcal{I}_{HO} than to \mathcal{I}_{HE} across CLIP, MoCo, and ConvNeXt features. This supports the interpretation that CLIP filtering over-selects canonical modes and under-covers harder variations.

Generator Quality and Data Budget Shift the Optimal Fidelity-Diversity Balance (α). We explore the relationship between α in Eq. 6 and different GMs. Our experiments use 1M synthetic CIFAR-10 samples from three GMs. As shown in Fig. 8, the optimal α depends on both the quality of the synthetic data and the volume of training data. (1) For StyleGAN2 (Fig. 8a), which yields the highest FID, fidelity remains the key factor for classification performance; (2) When the generated distributions are closer to the real (as in EDM and EDM2), Figs.8b, 8c demonstrate the benefit of

Table 4: Similarity of high-CLIP data to $\mathcal{I}_{HO}/\mathcal{I}_{HE}$.

Set	CLIP	MoCo	ConvNeXt
\mathcal{I}_{HO}	0.946	0.934	0.839
\mathcal{I}_{HE}	0.943	0.914	0.805

Table 5: Curation steps overhead across real data sizes.

Stage	10K	100K	1M
Feat. Ext. (Min.)	65.07	65.71	75.55
$\mathcal{I}_{HO}/\mathcal{I}_{HE}$ split (Sec.)	0.51	1.06	18.42
Score & Select (Sec.)	5.41	80.10	821.81

Table 6: Compute-accuracy trade-off in Eff.Net-B0 (1 × NVIDIA L40S).

Ours vs. Rand	Duration↓(Min.)	Accuracy↑ (%)
200K vs. 300K	83.8 vs. 120.0	75.03 vs. 74.59
300K vs. 500K	123.8 vs. 210.0	75.91 vs. 75.70

tuning the trade-off factor α . (3) Arcross all the datasets, as the training volume increases, the optimal α shifts toward larger values, underscoring the increasing importance of diversity at larger scales, where canonical high-fidelity samples provide limited additional gains. (4) In terms of the best α in each GMs, the biggest shift is observed in the most advanced EDM2, suggesting that with larger training volumes and highly realistic generations, diversity becomes the decisive factor.

Impact of Feature Extractors. Since our strategy relies on image features, we examine whether the choice of feature extractor matters. We conduct an ablation study using three representative encoders, each reflecting a distinct training paradigm: SigLIP (text-image alignment) [73], DINOv3 (self-supervised) [74], and ViT (supervised). Evaluations are performed on two datasets with different image resolutions, CIFAR-10 and ImageNet-100 (configurations are summarized in Appendix F.2). The results, summarized in Fig. 9, show that although SigLIP achieves the best performance, the absolute differences among extractors remain modest. This suggests that SigLIP is a promising choice, but its impact is relatively minor compared to the quality of synthetic data and the choice of α in the proposed strategy.

Curation Overhead Is Small Relative to Training. Comparing to previous post-generation selection, our curation introduces unique cost in $\mathcal{I}_{HO}/\mathcal{I}_{HE}$ splitting, scoring and selection. Once features are extracted, all such operations reduce to batched cosine similarity computations that are GPU-friendly and fast in practice (implementation in Appendix G.1, G.2). Tab. 5 shows the runtime of each stage of our curation for 10M synthetic samples across varying real-data scales. Feature extraction dominates the overall overhead. Since it is a one-time inference cost shared by most instance-selection baselines, the overhead specific to our method remains negligible even at large scales.

Furthermore, when downstream training is considered, the extra curation cost is well justified. In the Tiny-ImageNet setting, curation of a 1M-image pool takes 3.8 minutes in total (3.5 minutes for feature extraction and 0.3 minutes for scoring and selection). In contrast, training on 200K, 300K, and 500K augmented samples takes 80, 120, and 210 minutes, respectively. As shown in Tab. 6, despite incurring 3.8 additional minutes over random selection, our method delivers better performance with fewer training samples, effectively compensating for the curation overhead in downstream training.

The Characteristics of HO-HE Split in Real Data. Splitting \mathcal{I}_{HO} and \mathcal{I}_{HE} within a class across datasets, the number of samples in each subset remains nearly equal, suggesting that *approximately half of the samples effectively capture the primary semantics of the class*. Using \mathcal{I}_{HO} and \mathcal{I}_{HE} as curation references, we observed that although the two sets have comparable volumes, \mathcal{I}_{HO} yields fewer unique synthetic instances. We attribute this to the *higher intra-class similarity within \mathcal{I}_{HO}* (Tab. 7 in the Appendix), which makes it more challenging for GMs to capture fine-grained variations among similar concepts, compared to the more diverse \mathcal{I}_{HE} .

6 Conclusions

We introduced a generator-agnostic framework for post-generation curation of synthetic images. By splitting real data into HO and HE references and selecting synthetics with a partition-wise fidelity-diversity score, the method improves in-domain accuracy, strengthens OOD generalization, reduces the amount of synthetic data needed to match real-data baselines, and remains complementary to task-customized generation for both classification and segmentation. The analysis further suggests a practical principle for synthetic-data use: as generator fidelity and training budgets increase, curation should shift from merely retaining recognizable samples toward allocating more budget to non-redundant variation.

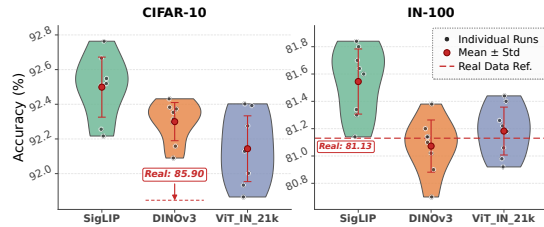


Figure 9: Testing accuracy of models trained on selected synthetic data with different feature extractors. The corresponding training configurations are provided in Appendix F.2.

References

- [1] Chenyu Zheng, Guoqiang Wu, and Chongxuan Li. Toward understanding generative data augmentation. In *Thirty-seventh Conference on Neural Information Processing Systems*, 2023. URL <https://openreview.net/forum?id=W5C1q1bSrR>.
- [2] Mert Bulent Sariyildiz, Karteek Alahari, Diane Larlus, and Yannis Kalantidis. Fake it till you make it: Learning transferable representations from synthetic imagenet clones. In *Proceedings of the IEEE/CVF Conference on Computer Vision and Pattern Recognition (CVPR)*, pages 8011–8021, 2023.
- [3] Shekoofeh Azizi, Simon Kornblith, Chitwan Saharia, Mohammad Norouzi, and David J. Fleet. Synthetic data from diffusion models improves imagenet classification. *Transactions on Machine Learning Research*, 2023. ISSN 2835-8856. URL <https://openreview.net/forum?id=D1RsoxjyPm>.
- [4] Ruifei He, Shuyang Sun, Xin Yu, Chuhui Xue, Wenqing Zhang, Philip Torr, Song Bai, and Xiaojuan Qi. Is synthetic data from generative models ready for image recognition? In *The Eleventh International Conference on Learning Representations*, 2023. URL <https://openreview.net/forum?id=nUmCcZ5RKF>.
- [5] Yuhang Li, Xin Dong, Chen Chen, Jingtao Li, Yuxin Wen, Michael Spranger, and Lingjuan Lyu. IS SYNTHETIC DATA USEFUL FOR TRANSFER LEARNING? AN INVESTIGATION INTO DATA GENERATION, VOLUME, AND UTILIZATION, 2024. URL <https://openreview.net/forum?id=CjPt1AC6w0>.
- [6] Lijie Fan, Kaifeng Chen, Dilip Krishnan, Dina Katabi, Phillip Isola, and Yonglong Tian. Scaling laws of synthetic images for model training ... for now. In *CVPR*, pages 7382–7392, 2024. URL <https://doi.org/10.1109/CVPR52733.2024.00705>.
- [7] Jae Myung Kim, Jessica Bader, Stephan Alaniz, Cordelia Schmid, and Zeynep Akata. Datadream: Few-shot guided dataset generation. In *European Conference on Computer Vision*, pages 252–268. Springer, 2024.
- [8] Jianhao Yuan, Jie Zhang, Shuyang Sun, Philip Torr, and Bo Zhao. Real-fake: Effective training data synthesis through distribution matching, 2024. URL <https://arxiv.org/abs/2310.10402>.
- [9] Sunwoo Kim, Minkyu Kim, and Dongmin Park. Test-time alignment of diffusion models without reward over-optimization. *arXiv preprint arXiv:2501.05803*, 2025.
- [10] Yijun Liang, Shweta Bhardwaj, and Tianyi Zhou. Diffusion curriculum: Synthetic-to-real data curriculum via image-guided diffusion. In *Proceedings of the IEEE/CVF International Conference on Computer Vision*, pages 1697–1707, 2025.
- [11] Nicola Dall’Asen, Xiaofeng Zhang, Reyhane Askari Hemmat, Melissa Hall, Jakob Verbeek, Adriana Romero-Soriano, and Michal Drozdal. Increasing the utility of synthetic images through chamfer guidance. *arXiv preprint arXiv:2508.10631*, 2025.
- [12] Michael Kirchhof, James Thornton, Louis Béthune, Pierre Ablin, Eugene Ndiaye, and Marco Cuturi. Shielded diffusion: Generating novel and diverse images using sparse repellency. *arXiv preprint arXiv:2410.06025*, 2024.
- [13] Jordan Shipard, Arnold Wiliem, Kien Nguyen Thanh, Wei Xiang, and Clinton Fookes. Diversity is definitely needed: Improving model-agnostic zero-shot classification via stable diffusion. In *2023 IEEE/CVF Conference on Computer Vision and Pattern Recognition Workshops (CVPRW)*, page 769–778. IEEE, June 2023. doi: 10.1109/cvprw59228.2023.00084. URL <http://dx.doi.org/10.1109/CVPRW59228.2023.00084>.
- [14] Fazle Rahat, M Shifat Hossain, Md Rubel Ahmed, Sumit Kumar Jha, and Rickard Ewetz. Data augmentation for image classification using generative ai. In *2025 IEEE/CVF Winter Conference on Applications of Computer Vision (WACV)*, pages 4173–4182. IEEE, 2025.

- [15] Lisa Dunlap, Alyssa Umno, Han Zhang, Jiezhi Yang, Joseph E. Gonzalez, and Trevor Darrell. Diversify your vision datasets with automatic diffusion-based augmentation. In *Thirty-seventh Conference on Neural Information Processing Systems*, 2023. URL <https://openreview.net/forum?id=9wrYfqdrwk>.
- [16] Samir Yitzhak Gadre, Gabriel Ilharco, Alex Fang, Jonathan Hayase, Georgios Smyrnis, Thao Nguyen, Ryan Marten, Mitchell Wortsman, Dhruva Ghosh, Jieyu Zhang, Eyal Orgad, Rahim Entezari, Giannis Daras, Sarah M Pratt, Vivek Ramanujan, Yonatan Bitton, Kalyani Marathe, Stephen Mussmann, Richard Vencu, Mehdi Cherti, Ranjay Krishna, Pang Wei Koh, Olga Saukh, Alexander Ratner, Shuran Song, Hannaneh Hajishirzi, Ali Farhadi, Romain Beaumont, Sewoong Oh, Alex Dimakis, Jenia Jitsev, Yair Carmon, Vaishaal Shankar, and Ludwig Schmidt. Datacomp: In search of the next generation of multimodal datasets. In *Thirty-seventh Conference on Neural Information Processing Systems Datasets and Benchmarks Track*, 2023. URL <https://openreview.net/forum?id=dVaWCDMBof>.
- [17] Amro Abbas, Kushal Tirumala, Dániel Simig, Surya Ganguli, and Ari S Morcos. Semd-edup: Data-efficient learning at web-scale through semantic deduplication. *arXiv preprint arXiv:2303.09540*, 2023.
- [18] Yunhao Chen, Yunjie Zhu, Zihui Yan, Zhen Ren, Yifan Huang, Jianlu Shen, and Lifang Chen. Effective audio classification network based on paired inverse pyramid structure and dense mlp block. In *International Conference on Intelligent Computing*, pages 70–84. Springer, 2023.
- [19] Yuxuan Zhang, Huan Ling, Jun Gao, Kangxue Yin, Jean-Francois Lafleche, Adela Barriuso, Antonio Torralba, and Sanja Fidler. Datasetgan: Efficient labeled data factory with minimal human effort. In *Proceedings of the IEEE/CVF Conference on Computer Vision and Pattern Recognition*, pages 10145–10155, 2021.
- [20] Tuomas Kynkäänniemi, Tero Karras, Samuli Laine, Jaakko Lehtinen, and Timo Aila. Improved precision and recall metric for assessing generative models. In H. Wallach, H. Larochelle, A. Beygelzimer, F. d'Alché-Buc, E. Fox, and R. Garnett, editors, *Advances in Neural Information Processing Systems*, volume 32. Curran Associates, Inc., 2019. URL https://proceedings.neurips.cc/paper_files/paper/2019/file/0234c510bc6d908b28c70ff313743079-Paper.pdf.
- [21] Shaobo Lin, Kun Wang, Xingyu Zeng, and Rui Zhao. Explore the power of synthetic data on few-shot object detection. In *Proceedings of the IEEE/CVF conference on computer vision and pattern recognition*, pages 638–647, 2023.
- [22] Datao Tang, Xiangyong Cao, Xuan Wu, Jialin Li, Jing Yao, Xueru Bai, Dongsheng Jiang, Yin Li, and Deyu Meng. Aerogen: Enhancing remote sensing object detection with diffusion-driven data generation. In *Proceedings of the Computer Vision and Pattern Recognition Conference*, pages 3614–3624, 2025.
- [23] Kunpeng Qiu, Zhiqiang Gao, Zhiying Zhou, Mingjie Sun, and Yongxin Guo. Noise-consistent siamese-diffusion for medical image synthesis and segmentation. In *Proceedings of the Computer Vision and Pattern Recognition Conference*, pages 15672–15681, 2025.
- [24] Yinong Oliver Wang, Younjoon Chung, Chen Henry Wu, and Fernando De la Torre. Domain gap embeddings for generative dataset augmentation. In *Proceedings of the IEEE/CVF Conference on Computer Vision and Pattern Recognition*, pages 28684–28694, 2024.
- [25] Yongchao Zhou, Hshmat Sahak, and Jimmy Ba. Training on thin air: Improve image classification with generated data, 2023. URL <https://arxiv.org/abs/2305.15316>.
- [26] Yonglong Tian, Lijie Fan, Phillip Isola, Huiwen Chang, and Dilip Krishnan. Stablerep: Synthetic images from text-to-image models make strong visual representation learners, 2023. URL <https://arxiv.org/abs/2306.00984>.
- [27] Hasan Abed Al Kader Hammoud, Hani Itani, Fabio Pizzati, Philip Torr, Adel Bibi, and Bernard Ghanem. Synthclip: Are we ready for a fully synthetic clip training?, 2024. URL <https://arxiv.org/abs/2402.01832>.

- [28] Yonglong Tian, Lijie Fan, Kaifeng Chen, Dina Katabi, Dilip Krishnan, and Phillip Isola. Learning vision from models rivals learning vision from data, 2023. URL <https://arxiv.org/abs/2312.17742>.
- [29] Dewen Zeng, Yawen Wu, Xinrong Hu, Xiaowei Xu, and Yiyu Shi. Contrastive learning with synthetic positives, 2025. URL <https://arxiv.org/abs/2408.16965>.
- [30] Maan Qraitem, Kate Saenko, and Bryan A. Plummer. From fake to real: Pretraining on balanced synthetic images to prevent spurious correlations in image recognition, 2024. URL <https://arxiv.org/abs/2308.04553>.
- [31] Ryuichiro Hataya, Han Bao, and Hiromi Arai. Will large-scale generative models corrupt future datasets? In *2023 IEEE/CVF International Conference on Computer Vision (ICCV)*, page 20498–20508. IEEE, October 2023. doi: 10.1109/iccv51070.2023.01879. URL <http://dx.doi.org/10.1109/ICCV51070.2023.01879>.
- [32] Yifei Wang, Jizhe Zhang, and Yisen Wang. Do generated data always help contrastive learning?, 2024. URL <https://arxiv.org/abs/2403.12448>.
- [33] Jiyu Guo, Shuo Yang, Yiming Huang, Yancheng Long, Xiaobo Xia, Xiu Su, Bo Zhao, Zeke Xie, and Liqiang Nie. Utilgen: Utility-centric generative data augmentation with dual-level task adaptation. In *The Thirty-ninth Annual Conference on Neural Information Processing Systems*, 2026. URL <https://openreview.net/forum?id=tBQEPRFT60>.
- [34] Amro Abbas, Evgenia Rusak, Kushal Tirumala, Wieland Brendel, Kamalika Chaudhuri, and Ari S Morcos. Effective pruning of web-scale datasets based on complexity of concept clusters. *arXiv preprint arXiv:2401.04578*, 2024.
- [35] Shivam Chandhok, Qian Yang, Oscar Mañas, Kanishk Jain, Leonid Sigal, and Aishwarya Agrawal. Learning what matters: Prioritized concept learning via relative error-driven sample selection. *arXiv preprint arXiv:2506.01085*, 2025.
- [36] Binod Bhattarai, Seungryul Baek, Rumeysa Bodur, and Tae-Kyun Kim. Sampling strategies for gan synthetic data. In *ICASSP 2020 - 2020 IEEE International Conference on Acoustics, Speech and Signal Processing (ICASSP)*, page 2303–2307. IEEE, May 2020. doi: 10.1109/icassp40776.2020.9054677. URL <http://dx.doi.org/10.1109/ICASSP40776.2020.9054677>.
- [37] Yuxuan Zhang, Huan Ling, Jun Gao, Kangxue Yin, Jean-Francois Lafleche, Adela Barriuso, Antonio Torralba, and Sanja Fidler. Datasetgan: Efficient labeled data factory with minimal human effort. In *2021 IEEE/CVF Conference on Computer Vision and Pattern Recognition (CVPR)*, page 10140–10150. IEEE, June 2021. doi: 10.1109/cvpr46437.2021.01001. URL <http://dx.doi.org/10.1109/CVPR46437.2021.01001>.
- [38] Yunhao Chen, Zihui Yan, Yunjie Zhu, Zhen Ren, Jianlu Shen, and Yifan Huang. Data augmentation for environmental sound classification using diffusion probabilistic model with top-k selection discriminator. In *International Conference on Intelligent Computing*, pages 283–295. Springer, 2023.
- [39] Tu Vu, Minh-Thang Luong, Quoc Le, Grady Simon, and Mohit Iyyer. Strata: Self-training with task augmentation for better few-shot learning. In *Proceedings of the 2021 Conference on Empirical Methods in Natural Language Processing*. Association for Computational Linguistics, 2021. doi: 10.18653/v1/2021.emnlp-main.462. URL <http://dx.doi.org/10.18653/v1/2021.emnlp-main.462>.
- [40] Alec Radford, Jong Wook Kim, Chris Hallacy, Aditya Ramesh, Gabriel Goh, Sandhini Agarwal, Girish Sastry, Amanda Askell, Pamela Mishkin, Jack Clark, Gretchen Krueger, and Ilya Sutskever. Learning transferable visual models from natural language supervision. In Marina Meila and Tong Zhang, editors, *Proceedings of the 38th International Conference on Machine Learning*, volume 139 of *Proceedings of Machine Learning Research*, pages 8748–8763. PMLR, 18–24 Jul 2021. URL <https://proceedings.mlr.press/v139/radford21a.html>.
- [41] Hao Tang, Siyue Yu, Jian Pang, and Bingfeng Zhang. A training-free synthetic data selection method for semantic segmentation, 2025. URL <https://arxiv.org/abs/2501.15201>.

- [42] Muhammad Ferjad Naeem, Seong Joon Oh, Youngjung Uh, Yunjey Choi, and Jaejun Yoo. Reliable fidelity and diversity metrics for generative models, 2020.
- [43] Dong Chen, Xinda Qi, Yu Zheng, Yuzhen Lu, Yanbo Huang, and Zhaojian Li. Deep data augmentation for weed recognition enhancement: A diffusion probabilistic model and transfer learning based approach. In *2023 ASABE Annual International Meeting*, page 1. American Society of Agricultural and Biological Engineers, 2023.
- [44] Victor G Turrisi da Costa, Nicola Dall’Asen, Yiming Wang, Nicu Sebe, and Elisa Ricci. Diversified in-domain synthesis with efficient fine-tuning for few-shot classification. *arXiv preprint arXiv:2312.03046*, 2023.
- [45] Brandon Trabucco, Kyle Doherty, Max A Gurinas, and Ruslan Salakhutdinov. Effective data augmentation with diffusion models. In *The Twelfth International Conference on Learning Representations*, 2024. URL <https://openreview.net/forum?id=ZWzUA9zeAg>.
- [46] Reyhane Askari Hemmat, Mohammad Pezeshki, Florian Bordes, Michal Drozdal, and Adriana Romero-Soriano. Feedback-guided data synthesis for imbalanced classification, 2024. URL <https://arxiv.org/abs/2310.00158>.
- [47] Xinlei Chen*, Saining Xie*, and Kaiming He. An empirical study of training self-supervised vision transformers. *arXiv preprint arXiv:2104.02057*, 2021.
- [48] Yuval Netzer, Tao Wang, Adam Coates, Alessandro Bissacco, Bo Wu, and Andrew Y. Ng. Reading digits in natural images with unsupervised feature learning. In *NIPS Workshop on Deep Learning and Unsupervised Feature Learning 2011*, 2011. URL http://ufldl.stanford.edu/housenumbers/nips2011_housenumbers.pdf.
- [49] Alex Krizhevsky, Vinod Nair, and Geoffrey Hinton. Cifar-10 (canadian institute for advanced research). URL <http://www.cs.toronto.edu/kriz/cifar.html>, 5(4):1, 2010.
- [50] Ya Le and Xuan S. Yang. Tiny imagenet visual recognition challenge. 2015. URL <https://api.semanticscholar.org/CorpusID:16664790>.
- [51] Zekai Wang, Tianyu Pang, Chao Du, Min Lin, Weiwei Liu, and Shuicheng Yan. Better diffusion models further improve adversarial training. In *International Conference on Machine Learning (ICML)*, 2023.
- [52] Tero Karras, Miika Aittala, Jaakko Lehtinen, Janne Hellsten, Timo Aila, and Samuli Laine. Analyzing and improving the training dynamics of diffusion models. In *Proc. CVPR*, 2024.
- [53] Tero Karras, Miika Aittala, Tuomas Kynkäänniemi, Jaakko Lehtinen, Timo Aila, and Samuli Laine. Guiding a diffusion model with a bad version of itself. In *Proc. NeurIPS*, 2024.
- [54] Yonglong Tian, Dilip Krishnan, and Phillip Isola. Contrastive multiview coding. In *European conference on computer vision*, pages 776–794. Springer, 2020.
- [55] Mark Everingham, S. M. Ali Eslami, Luc Van Gool, Christopher K. I. Williams, John Winn, and Andrew Zisserman. The pascal visual object classes challenge: A retrospective. *International Journal of Computer Vision*, 111(1):98–136, 2015.
- [56] Erroll Wood, Tadas Baltrušaitis, Charlie Hewitt, Sebastian Dziadzio, Matthew Johnson, Virginia Estellers, Thomas J. Cashman, and Jamie Shotton. Fake it till you make it: Face analysis in the wild using synthetic data alone, 2021. URL <https://arxiv.org/abs/2109.15102>.
- [57] Nicolas Carlini, Jamie Hayes, Milad Nasr, Matthew Jagielski, Vikash Sehwal, Florian Tramer, Borja Balle, Daphne Ippolito, and Eric Wallace. Extracting training data from diffusion models. In *32nd USENIX Security Symposium (USENIX Security 23)*, pages 5253–5270, 2023.
- [58] Minchul Kim, Feng Liu, Anil Jain, and Xiaoming Liu. Dcface: Synthetic face generation with dual condition diffusion model. In *Proceedings of the IEEE/CVF conference on computer vision and pattern recognition*, pages 12715–12725, 2023.

- [59] Reyhane Askari Hemmat, Melissa Hall, Alicia Sun, Candace Ross, Michal Drozdal, and Adriana Romero-Soriano. Improving geo-diversity of generated images with contextualized vendi score guidance. In *European Conference on Computer Vision*, pages 213–229. Springer, 2024.
- [60] Haoyu Wang, Lei Zhang, Wenrui Liu, Dengyang Jiang, Wei Wei, and Chen Ding. Jodiffusion: Jointly diffusing image with pixel-level annotations for semantic segmentation promotion. In *Proceedings of the AAAI Conference on Artificial Intelligence*, volume 40, pages 9775–9783, 2026.
- [61] Kaiming He, Xiangyu Zhang, Shaoqing Ren, and Jian Sun. Deep residual learning for image recognition. In *Proceedings of the IEEE conference on computer vision and pattern recognition*, pages 770–778, 2016.
- [62] Mingxing Tan and Quoc Le. Efficientnet: Rethinking model scaling for convolutional neural networks. In *International conference on machine learning*, pages 6105–6114. PMLR, 2019.
- [63] Bichen Wu, Chenfeng Xu, Xiaoliang Dai, Alvin Wan, Peizhao Zhang, Zhicheng Yan, Masayoshi Tomizuka, Joseph Gonzalez, Kurt Keutzer, and Peter Vajda. Visual transformers: Token-based image representation and processing for computer vision, 2020.
- [64] Dan Hendrycks and Thomas Dietterich. Benchmarking neural network robustness to common corruptions and perturbations. In *International Conference on Learning Representations*, 2019. URL <https://openreview.net/forum?id=HJz6tiCqYm>.
- [65] Benjamin Recht, Rebecca Roelofs, Ludwig Schmidt, and Vaishal Shankar. Do imagenet classifiers generalize to imagenet?, 2019. URL <https://arxiv.org/abs/1902.10811>.
- [66] Haohan Wang, Songwei Ge, Zachary Lipton, and Eric P Xing. Learning robust global representations by penalizing local predictive power. In *Advances in Neural Information Processing Systems*, pages 10506–10518, 2019.
- [67] Dan Hendrycks and Thomas Dietterich. Benchmarking neural network robustness to common corruptions and perturbations. *Proceedings of the International Conference on Learning Representations*, 2019.
- [68] Tiago Salvador and Adam M Oberman. Imagenet-cartoon and imagenet-drawing: two domain shift datasets for imagenet. In *ICML 2022 Shift Happens Workshop*, 2022. URL <https://openreview.net/forum?id=YLAUXhjwaQt>.
- [69] Xiaoxiao Sun, Xingjian Leng, Zijian Wang, Yang Yang, Zi Huang, and Liang Zheng. Cifar-10-warehouse: Broad and more realistic testbeds in model generalization analysis. In *ICLR*, 2024.
- [70] Liang-Chieh Chen, Yukun Zhu, George Papandreou, Florian Schroff, and Hartwig Adam. Encoder-decoder with atrous separable convolution for semantic image segmentation. In *Proceedings of the European conference on computer vision (ECCV)*, pages 801–818, 2018.
- [71] Tero Karras, Miika Aittala, Janne Hellsten, Samuli Laine, Jaakko Lehtinen, and Timo Aila. Training generative adversarial networks with limited data. In *Proc. NeurIPS*, 2020.
- [72] Tero Karras, Miika Aittala, Timo Aila, and Samuli Laine. Elucidating the design space of diffusion-based generative models. In *Proc. NeurIPS*, 2022.
- [73] Xiaohua Zhai, Basil Mustafa, Alexander Kolesnikov, and Lucas Beyer. Sigmoid loss for language image pre-training, 2023.
- [74] Oriane Siméoni, Huy V. Vo, Maximilian Seitzer, Federico Baldassarre, Maxime Oquab, Cijo Jose, Vasil Khalidov, Marc Szafraniec, Seungeun Yi, Michaël Ramamonjisoa, Francisco Massa, Daniel Haziza, Luca Wehrstedt, Jianyuan Wang, Timothée Darcet, Théo Moutakanni, Leonel Sentana, Claire Roberts, Andrea Vedaldi, Jamie Tolan, John Brandt, Camille Couprie, Julien Mairal, Hervé Jégou, Patrick Labatut, and Piotr Bojanowski. Dinov3, 2025.
- [75] Ross Wightman. Pytorch image models. <https://github.com/rwightman/pytorch-image-models>, 2019.

Appendix

The supplementary material is organized by the role each section plays in supporting the main paper. Appendix A first gives visual examples and intra-class statistics that characterize the HO/HE partition. Appendix B explains the motivation and theoretical interpretation of the partition. Appendix C examines how the HO/HE split exposes generator and discriminator biases. Appendix D describes the synthetic-data selection procedure and visualizes the diversity score. Appendix E provides the full experimental details, including compute resources, generator usage, training recipes, in-domain results, and out-of-domain results. Appendix F reports additional ablations, Appendix G gives the scoring and selection implementation, and Appendices H–I discuss limitations and broader impacts.

A Visual and Statistical Properties of the HO/HE Partition

This section provides the visual and quantitative evidence referenced in Sec. 3.1. We partition each real class into \mathcal{I}_{HO} , which contains local canonical representatives, and \mathcal{I}_{HE} , which contains less redundant intra-class variation. Fig. 10 shows CIFAR-10 examples, and Tab. 7 shows that \mathcal{I}_{HO} has higher intra-class similarity than \mathcal{I}_{HE} across datasets.

Table 7: Average intra-class similarity of \mathcal{I}_{HO} and \mathcal{I}_{HE} across datasets. \mathcal{I}_{HO} consistently gets higher intra-class similarity.

Subset	SVHN	CIFAR-10	Tiny-ImageNet	ImageNet-1K
\mathcal{I}_{HO}	0.8507	0.7948	0.8236	0.8000
\mathcal{I}_{HE}	0.8385	0.7887	0.7894	0.7725

B Motivation and Theoretical Justification of HO-HE Partition

In Sec. 3.1, we argue that the proposed HO-HE partition admits a theoretical justification under a graph-based view. In this section, we further elaborate the motivation behind the HO and HE design and provide a formal analysis showing why optimizing with respect to this partition is well-aligned with the learning objective in our setting.

B.1 Semantic-mode diversity and Variation Diversity

To clarify the design of our real data partition, we first distinguish between semantic-mode diversity and variation diversity. We provide a PCA visualization in Figure 11. In Figure 11a, the real data are partitioned into two sets based on the distance of each instance to the class centroid: the “near” set contains canonical patterns, while the “far” set consists of patterns that are less similar to the semantic core and therefore exhibit higher semantic-mode diversity. Each of them cover the subregion of original feature space. In contrast, Figure 11b illustrates our HO/HE partition, where both HO and HE cover all semantic modes present in the real data, and the diversity in HE manifests as variation diversity, rich variations around each semantic mode across the entire dataset.

Thus, Figure 11a illustrates semantic-mode diversity: the “near” and “far” sets are distinguished by the presence of different semantic modes in each subregion. In contrast, Figure 11b shows the HO/HE partition, where the two sets are distinguished by the variation level within each mode across the entire feature space, rather than by different modes themselves.

B.2 Why we choose HO-HE PARTITION

Standard image augmentations improve model performance by increasing variation within the dataset while preserving the main semantics. Inspired by this, we hypothesize that, when curating synthetic data, if we can construct a set that covers all semantic modes while exhibiting high variation within each mode, we can similarly expect performance gains. Based on this idea, we propose the HO/HE partition of the real data, which preserves all modes (as shown in Figure 11b) but explicitly distinguishes them by their level of intra-mode variation, and use them as guidance for synthetic data selection.



Figure 10: For CIFAR-10, we select both HO and HE images within each class. HO instances (framed in blue) are more representative and better express the core semantics of given class. HE instances (framed in green) are more diverse, capturing a broader range of variations

B.3 Nearest-neighbor representative coverage

For each real feature r_i , define its nearest neighbor by

$$j(i) = \arg \min_{j \neq i} d(r_i, r_j).$$

The HO set is the image of this nearest-neighbor map, $H = \{r_{j(i)} : i \in [n]\}$, and the HE set is $E = R \setminus H$. Equivalently, if we build the directed 1-nearest-neighbor graph by drawing an edge $r_i \rightarrow r_{j(i)}$, then H is the set of nodes with positive in-degree and E is the set of zero in-degree nodes.

Proof of Proposition 1. For any r_i , the feature $r_{j(i)}$ belongs to H by construction and $j(i) \neq i$. Therefore

$$\min_{h \in H, h \neq r_i} d(r_i, h) \leq d(r_i, r_{j(i)}) = \min_{r \in R, r \neq r_i} d(r_i, r).$$

Since $H \subseteq R$, the reverse inequality holds automatically, giving equality for H .

Conversely, let $A \subseteq R$ satisfy the equality in Proposition 1 for every r_i . Under the unique-nearest-neighbor assumption, the only element of $R \setminus \{r_i\}$ that attains the right-hand side is $r_{j(i)}$. Hence $r_{j(i)} \in A$ for all i , and thus $H \subseteq A$. Since H itself satisfies the equality, it is the unique inclusion-minimal subset with this property.

Finally, set $\varepsilon = \max_i d(r_i, r_{j(i)})$. The equality just proved implies

$$\min_{h \in H, h \neq r_i} d(r_i, h) = d(r_i, r_{j(i)}) \leq \varepsilon$$

for every $r_i \in R$, yielding the stated coverage radius. \square

This result gives the precise sense in which HO contains canonical representatives: it is the smallest set that preserves every training point’s nearest-neighbor reconstruction cost. The complement HE is therefore not “noise” or “outliers” by definition; rather, it contains real samples that are not needed as nearest-neighbor representatives for other samples and thus encode less redundant local variation.

B.4 Geometric interpretation of the diversity score.

The diversity score has a simple angular meaning. For an HE anchor r , let $a_r = h(r) - r$ be the direction from r to its nearest HO neighbor. If a synthetic candidate z moves from r inside a cone of half-angle θ around a_r , then

$$\left\langle \frac{z - r}{\|z - r\|}, \frac{a_r}{\|a_r\|} \right\rangle \geq \cos \theta \quad \Rightarrow \quad S_{\text{div}}^{\text{HE}}(z, r) \leq -\cos \theta.$$

Thus increasing α suppresses candidates that are close to an HE anchor only by drifting back toward the canonical HO direction. This is the intended complement to the fidelity term: fidelity keeps the selected sample semantically aligned with an anchor, while diversity discourages repeated canonical collapse.

B.5 Graph interpretation of the HO-HE partition.

In this section, we discuss the properties of the HO-HE partition and prove its optimality in our setting. As defined HO-HE in Eqs. 2., we can review such partitions in the graph setting. In the original dataset, each feature of the image could be viewed as the node, and the cosine similarity between different features could be used as the distance connecting each pair of nodes (higher similarity corresponds to a smaller distance and less cost for transfer). Then we can compose a fully connected graph $G = (V, E)$, and V is the set of nodes, and $|V| = n$, and E is the set of edges, $|E| = n \times n$.

To find the “hubs” in the graph, we traverse all nodes in the graph and connect each node to its single nearest neighbor, forming a directed graph $G' = (V, E')$, where $|E'| = n$. Under this setting, HO is equivalent to the collection of nodes whose in-degree is positive.

So in the graph setting, the definition of HO could be rewritten as:

$$\text{HO} = \{a \in V \mid \exists b \in V \setminus \{a\}, \text{ such that } \forall c \in V \setminus \{a, b\}, d(a, b) \leq d(c, b)\}$$

Based on the definition above, we can derive the following properties:

1. To reach any node b in the graph, starting from a node in HO (different from b) consistently yields the minimal cost. Such property implies that learning the pattern in HO, and then we can reconstruct the whole original feature space with the smallest cost.
2. Suppose, in the original graph, each node has a single nearest neighbor. Then, theoretically, HO is a minimal subset of nodes such that every node in the graph can be reached from some node in HO with minimal cost.

Training downstream models on a given dataset can be interpreted as optimizing the model to capture the full set of patterns in the underlying feature space. From a graph perspective, once the model learns the patterns in HO, it can often propagate this knowledge to other nodes with relatively little

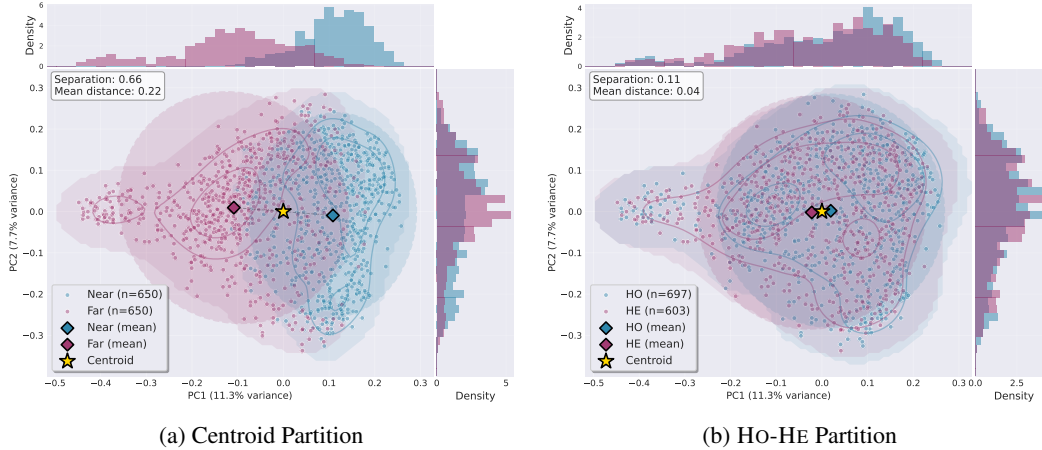


Figure 11: PCA visualization in ImageNet-1K (n03769881), using different partition strategies

additional cost. As a result, after sufficient training, downstream models naturally exhibit a preference for HO, where the patterns are easier to learn and generalize.

Therefore, motivated by this insight, we propose a synthetic data selection strategy built on the HO-HE partition to better unlock the value of synthetic samples for downstream training.

C Generator and Discriminator Biases in the HO/HE Split

Echoing the discussion of **Downstream Model Preference** in Sec. 3.1, \mathcal{I}_{HO} and \mathcal{I}_{HE} together constitute a complete real dataset, and when such data are used to train downstream models, these characteristics may be implicitly inherited.

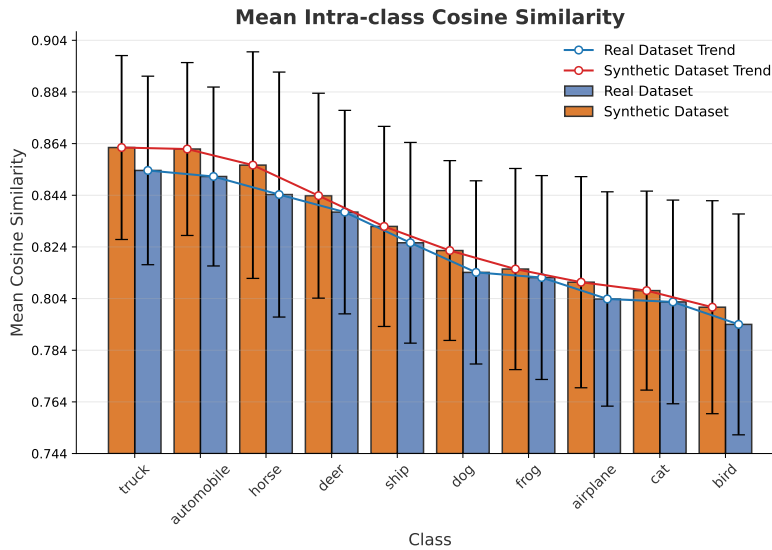


Figure 12: The cosine similarity measures how alike instances are within the individual class in CIFAR-10. From the figure, the mean cosine similarity of each class in the synthetic dataset follows the trend of the real dataset, indicating that the generative model effectively captures patterns from real data. However, the synthetic data consistently exhibit higher mean cosine similarity than the real data, suggesting that within each class, synthetic instances are more homogeneous and share greater similarity with each other compared to real instances. **This figure release that synthetic dataset have limitation of diversity in each individual class.**

For Generative Models, we investigate the relationship between generated instances and real instances in \mathcal{I}_{HO} and \mathcal{I}_{HE} . As shown in Figure 4, samples generated by EDM[72] exhibit higher similarity to those in the \mathcal{I}_{HO} , highlighting the well-known limitation of reduced diversity in generative data. Since \mathcal{I}_{HO} samples capture canonical patterns that are easier for generative models to learn, this bias toward \mathcal{I}_{HO} leads to higher intra-class similarity compared to real datasets, thereby reducing overall diversity, as shown in Figure 12.

For Discriminators, trained on real data, we observe a clear performance gap between \mathcal{I}_{HO} and \mathcal{I}_{HE} , even when evaluation is conducted on the original training set. As shown in Figure 13, we run inference using off-the-shelf pretrained models (referring Table 8) on the training datasets and consistently find higher accuracy on \mathcal{I}_{HO} than on \mathcal{I}_{HE} . We attribute this gap to differences in canonicity: \mathcal{I}_{HO} contains more canonical instances that are easier for models to fit, whereas \mathcal{I}_{HE} demands modeling a broader range of intra-class variations.

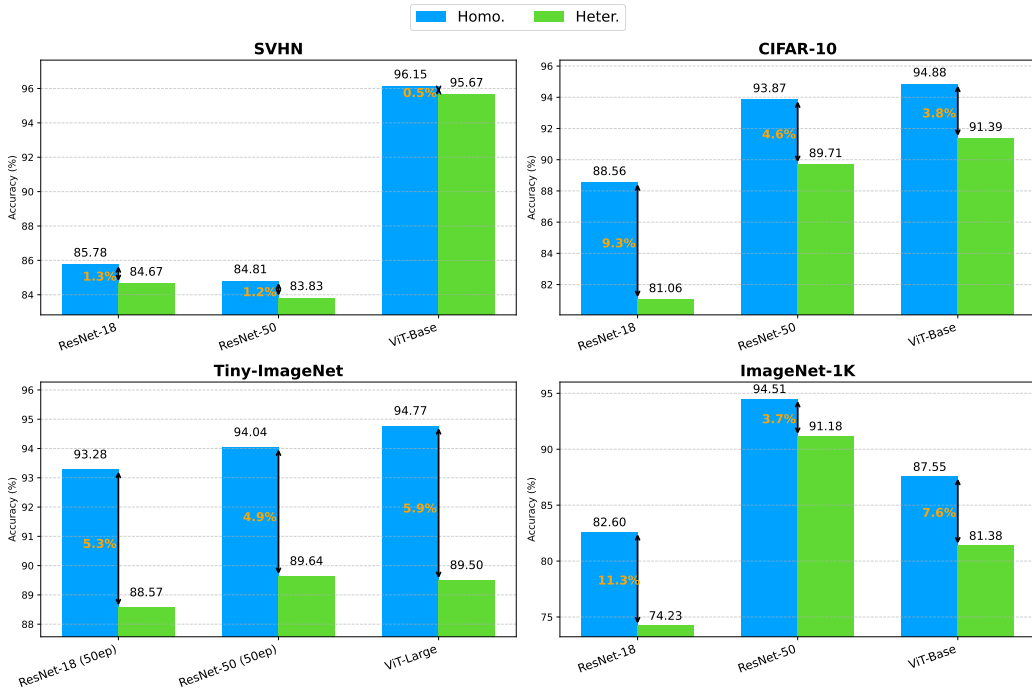


Figure 13: Performance gap between \mathcal{I}_{HO} and \mathcal{I}_{HE} across various datasets and pretrained models. For **SVHN**, **CIFAR-10**, **Tiny-ImageNet**, and **ImageNet-1K**, we evaluate multiple ResNet and ViT variants. Descriptions and links for all pretrained models are provided in Table 8. The experimental results reveal a striking fact: even within the training set, a clear performance gap persists between \mathcal{I}_{HO} and \mathcal{I}_{HE} .

Based on this observation, *training discriminators with generative data can be risky, as it may amplify the limitations already present in those trained with real data, further biasing the model toward canonical samples and degrading performance on real data inference.*

D Synthetic Data Selection Details

Following the previous discussion on HO and HE, this section introduces our synthetic data selection strategy designed to mitigate the limitations of training discriminators on generative data. The key difference from prior approaches is the incorporation of a diversity score. During selection, in addition to the fidelity score, which measures how closely synthetic samples resemble real data, the diversity score quantifies how far a synthetic instance departs from canonical patterns. As illustrated in Figure 14, when referencing real instances, a synthetic sample receives a higher diversity score if its direction from the HE set deviates more strongly from the direction toward the canonical pattern.

Table 8: Pretrained discriminators used in our experiments.

Dataset	Model	Link
SVHN	ResNet-18	https://huggingface.co/edadaltocg/resnet18_svhn
	ResNet-50	https://huggingface.co/edadaltocg/resnet50_svhn
	ViT-Base	https://huggingface.co/edadaltocg/vit_base_patch16_224_in21k_ft_svhn
CIFAR-10	ResNet-18	https://huggingface.co/SamAdamDay/resnet18_cifar10
	ResNet-50	https://huggingface.co/anonauthors/cifar10-timm-resnet50
	ViT-Base	https://huggingface.co/nateraw/vit-base-patch16-224-cifar10
Tiny-ImageNet	ResNet-18	https://github.com/zeyuanyin/tiny-imagenet
	ResNet-50	https://github.com/zeyuanyin/tiny-imagenet
	ViT-L	https://github.com/ehuynh1106/TinyImageNet-Transformers
ImageNet-1K	All models	timm [75]

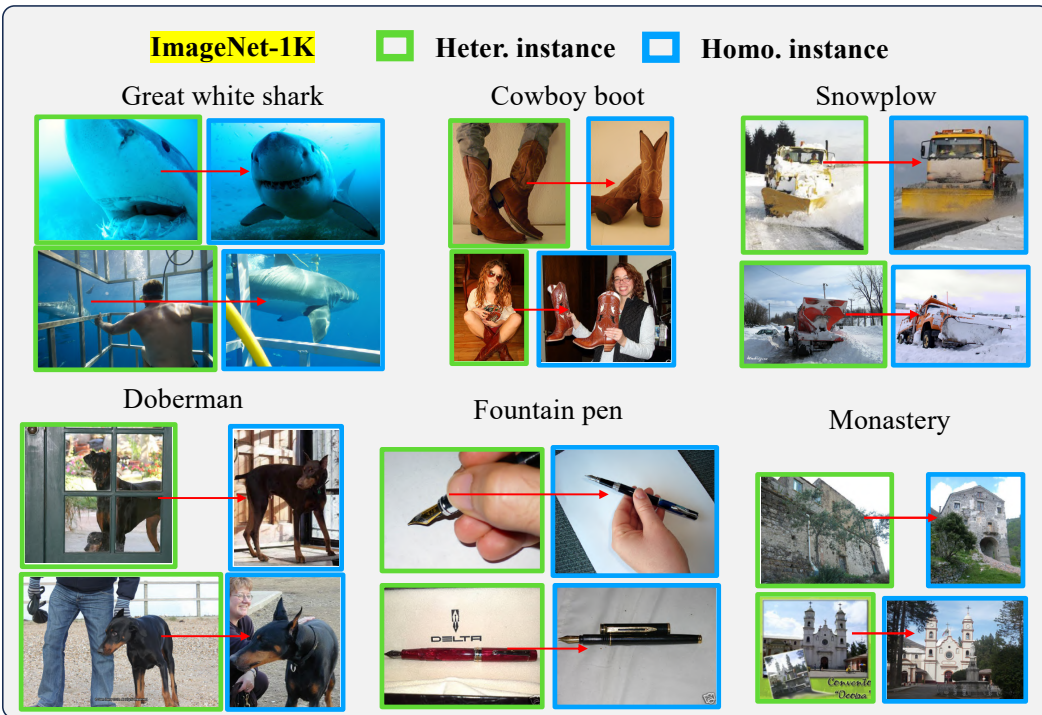


Figure 14: Examples of HE instances and their most similar counterparts in HO (based on MoCo V3 features) from ImageNet-1K. Red arrows denote vectors formed by each image pair. To capture the diversity within HE, our algorithm prioritizes synthetic images that, when paired with a **HE instance**, yield vectors that deviate from the red-arrow directions.

E Experiment Details and Full Results

E.1 Generator usage in the main paper

To validate our strategy, we train models on synthetic datasets and evaluate them on real data across two settings: in-domain and out-of-domain testing. In these experiments, we utilize publicly available generative models and synthetic dataset, and conduct training using their released code repositories. The corresponding responses are illustrated in Table 9. For the generator usage in Sec. 4.4, we follow the original papers and use the generators reported in [60, 59]

Table 9: Public repositories and resources used in this work. The first three rows correspond to classifier training repositories, and the last two rows correspond to generative models.

Resource	Link
Classifiers	
SVHN & CIFAR-10	https://github.com/ML-GSAI/Understanding-GDA
Tiny-ImageNet	https://github.com/DennisHanyuanXu/Tiny-ImageNet
ImageNet-1K	https://huggingface.co/docs/timm/training_script
Generative Models & Data	
Synthetic data & code for SVHN, CIFAR, and Tiny-ImageNet	https://github.com/wzekai99/DM-Improves-AT
Generator for ImageNet-1K	https://github.com/NVlabs/edm2

E.2 IN-1K training recipe

We use the timm codebase to train models for the IN-1K setting. Since training in IN-1K involves a relatively complex configuration and the final performance can vary with different settings, we report the exact configuration used in the main paper to facilitate reproduction of our empirical results. We train `vit_base_patch16_224` and `resnet50` from scratch, and fine-tune `vit_base_patch16_224.augreg_in21k` and `resnetv2_50x1_bit.goog_in21k` pretrained on ImageNet-21K. The concrete settings are shown in Figure 15.

Listing (1) ViT-B/16 training from scratch.

```
./distributed_train.sh "$NUM_GPU" \
--data-dir "$IMAGENET_DIR" \
--model vit_base_patch16_224 \
--epochs 120 --batch-size 256 \
--opt adamw --weight-decay 0.05 \
--sched cosine --warmup-epochs 5 \
--lr-base 5e-4 --lr-base-size 1024 \
--aa rand-m9-mstd0.5-inc1 \
--mixup 0.8 --cutmix 1.0 --smoothing 0.1 \
--drop-path 0.1 --channels-last --amp
```

Listing (2) ResNet-50 training from scratch.

```
./distributed_train.sh "$NUM_GPU" \
--data-dir "$IMAGENET_DIR" \
--model resnet50 \
--epochs 100 --batch-size 64 \
--opt sgd --momentum 0.9 --weight-decay 1e-4 \
--sched cosine --warmup-epochs 3
↪ --cooldown-epochs 10 \
--lr 0.025 --smoothing 0.1 \
--mixup 0.2 --cutmix 1.0 \
--aa rand-m9-mstd0.5-inc1 \
--drop-path 0.05 --amp --channels-last
```

Listing (3) Fine-tuning ViT-B/16 (IN-21K init).

```
./distributed_train.sh "$NUM_GPU" \
--data-dir "$IMAGENET_DIR" \
--model vit_base_patch16_224.augreg_in21k \
--pretrained \
--epochs 50 --batch-size 512 \
--opt adamw --weight-decay 0.05 \
--sched cosine --warmup-epochs 5 \
--lr-base 5e-5 --lr-base-size 1024 \
--aa rand-m9-mstd0.5-inc1 \
--mixup 0.2 --cutmix 0.8 --smoothing 0.1 \
--drop-path 0.1 --channels-last --amp
```

Listing (4) Fine-tuning ResNet-50 (IN-21K init).

```
./distributed_train.sh "$NUM_GPU" \
--data-dir "$IMAGENET_DIR" \
--model resnetv2_50x1_bit.goog_in21k \
--pretrained \
--epochs 50 --batch-size 64 \
--opt sgd --momentum 0.9 --weight-decay 1e-4 \
--sched cosine --warmup-epochs 3
↪ --cooldown-epochs 10 \
--lr 0.025 --smoothing 0.1 \
--mixup 0.2 --cutmix 1.0 \
--aa rand-m9-mstd0.5-inc1 \
--drop-path 0.05 --amp --channels-last
```

Figure 15: Training recipes for different backbones. Top row: from-scratch training. Bottom row: fine-tuning with ImageNet-21K initialization.

E.3 In-domain classification accuracy

Echoing Sec. 4.2, we evaluate model performance on SVHN, CIFAR-10, and Tiny-ImageNet to enable hierarchical assessment across datasets of varying complexity, and further conduct experiments on ImageNet-1K to simulate the large-scale setting.

SVHN: We compare our method with prior approaches, and the results are reported in Table 10. When trained exclusively on synthetic datasets, model performance can surpass that of models trained on real data as the training volume increases. Among different strategies, ours consistently achieves the best performance across varying training data scales.

Table 10: **ResNet18** performance on the **SVHN** dataset across different training sizes. As the amount of synthetic training data increases, model performance improves. The **green bold text** indicates the highest accuracy across different data selection strategies.

Method	73,257 (Ori. Size)	80K	90K	100K	200K	300K
<i>Real Data</i>	95.84±0.12	-	-	-	-	-
<i>RandSelect</i> [56]	94.65±0.11	94.95 ±0.16	95.03±0.20	95.04±0.13	95.78±0.08	96.28 ±0.13
<i>Clip-Align</i> [4]	89.14±0.31	89.38±0.26	89.67±0.23	89.67±0.17	90.22±0.24	90.70 ±0.22
<i>RealScore</i> [20]	94.60±0.12	95.03±0.18	95.03±0.13	95.20±0.16	95.72±0.13	96.20±0.05
<i>SBSim</i> [21]	94.71±0.16	95.13±0.08	95.22±0.12	95.25±0.14	95.84±0.13	96.16±0.06
<i>Ours</i>	95.44±0.17	95.59±0.12	95.66±0.11	95.83±0.13	96.33±0.11	96.65±0.04

CIFAR-10: We compare our method with prior approaches, and the results are reported in Table 11. When trained exclusively on synthetic datasets, model performance can surpass that of models trained on real data as the training volume increases. Among different strategies, ours consistently achieves the best performance across varying training data scales.

Table 11: **ResNet18** performance on the **CIFAR-10** dataset across different training sizes. As the amount of synthetic training data increases, model performance improves. The **green bold text** indicates the highest accuracy across different data selection strategies.

Methods	50K (Original Size)	70K	90K	100K	200K	300K	400K	500K
Real	85.80 ± 0.73	-	-	-	-	-	-	-
Random	84.57 ± 0.31	87.74 ±0.48	88.73 ±0.71	89.57±0.25	92.78±0.18	93.94±0.25	94.68 ±0.08	95.03±0.06
Clip	77.09±1.19	80.97±1.05	82.34±0.27	82.81±0.67	85.62±0.64	86.94±0.14	87.56±0.29	88.39±0.25
Realism	83.95±1.28	87.45±0.58	89.03±0.39	89.70±0.16	92.60±0.30	93.92±0.44	94.64±0.20	94.93±0.11
Similarity	84.67±0.98	87.12±0.70	88.72±0.38	89.41±0.23	91.79±0.23	93.21±0.17	93.83±0.17	94.23±0.13
<i>Ours</i>	84.96±0.31	87.90±0.35	89.66±0.40	90.47±0.39	93.43±0.17	94.86±0.20	95.45±0.16	95.71±0.10

Tiny-ImageNet: We compare our method with prior approaches, and the results are reported in Table 12. In this more complex setting, we first train models exclusively on synthetic data, where the performance gap between synthetic- and real-trained models is around 10%. To effectively validate the utility of synthetic data in discriminator training, we use synthetic data as an augmentation to real data. Under this setting, our method consistently outperforms alternatives across different experimental configurations.

Table 12: Performance of EfficientNet-B0 and Resnet50 on the **Tiny-ImageNet** dataset with different synthetic dataset. Results are reported as Mean ± Std. (relative difference from the real-data baseline). The best results in each column are highlighted. As the amount of synthetic training data increases, model performance improves. The experiment results demonstrate the importance of the trade-off between fidelity and diversity. The original data size is 100K.

	Data Selection Methods	+100K	+200K	+300K	+400K
EfficientNet-B0	<i>Real Data</i>	73.87 ± 0.29	-	-	-
	<i>RandSelect</i> [56]	74.16 ± 0.25 (+0.29)	74.59 ± 0.28 (+0.29)	75.00 ± 0.21 (+1.13)	75.70 ± 0.14 (+1.70)
	<i>CLIP-Align</i> [4]	60.54 ± 0.42 (-13.33)	62.24 ± 0.50 (-11.63)	62.59 ± 0.36 (-11.28)	63.13 ± 0.05 (-10.74)
	<i>RealScore</i> [20]	74.66 ± 0.27 (+0.79)	75.67 ± 0.19 (+1.90)	75.80 ± 0.14 (+1.93)	76.60 ± 0.04 (+2.73)
	<i>MaxSim</i> (α = 0) [21]	74.69 ± 0.09 (+0.82)	75.11 ± 0.25 (+1.24)	75.48 ± 0.29 (+1.61)	75.94 ± 0.16 (+2.07)
	<i>MaxDiv</i> (α = 1)	74.93 ± 0.11 (+1.06)	75.59 ± 0.11 (+1.72)	75.90 ± 0.11 (+2.03)	76.23 ± 0.05 (+2.36)
	<i>Ours</i>	75.03 ± 0.18 (+1.16)	75.91 ± 0.06 (+2.04)	76.65 ± 0.14 (+2.78)	76.86 ± 0.14 (+2.99)
ResNet-50	<i>Real Data</i>	64.13 ± 0.67	-	-	-
	<i>RandSelect</i> [56]	66.55 ± 0.24 (+2.42)	68.32 ± 0.25 (+4.19)	69.45 ± 0.42 (+5.32)	70.41 ± 0.21 (+6.28)
	<i>CLIP-Align</i> [4]	53.12 ± 0.88 (-11.01)	55.16 ± 0.38 (-8.97)	56.97 ± 0.30 (-7.16)	58.30 ± 0.25 (-5.83)
	<i>RealScore</i> [20]	66.05 ± 0.45 (+1.92)	69.12 ± 0.11 (+4.99)	70.09 ± 0.19 (+5.96)	71.51 ± 0.11 (+7.38)
	<i>SBSim</i> (α = 0) [21]	65.69 ± 0.35 (+1.56)	67.12 ± 0.57 (+2.99)	70.10 ± 0.37 (+5.97)	71.26 ± 0.42 (+7.13)
	<i>Diversity</i> (α = 1)	65.87 ± 0.50 (+1.74)	68.16 ± 0.25 (+4.03)	70.12 ± 0.13 (+5.99)	72.52 ± 0.21 (+8.39)
	<i>Ours</i>	68.57 ± 0.19 (+4.44)	70.82 ± 0.08 (+6.69)	71.80 ± 0.26 (+7.67)	73.05 ± 0.25 (+8.92)

E.4 Out-of-domain classification accuracy

Assessing models’ robustness, OOD evaluations are implemented (Sec. 4.3 in main paper). We report the concrete performance values in each setting as blow:

SVHN: We evaluate OOD performance using the extra split of SVHN [48] and test subset of distorted SVHN. Detailed results are presented in Table 13.

Table 13: **OOD** Performance comparison on **SVHN**. The best performance for each dataset is highlighted in **bold**.

Method	SVHN	SVHN-Extra	SVHN-test-small-collage	SVHN-test-middle-collage	SVHN-test-strong-collage	SVHN-test w/large-collage	SVHN-Extra w/large-collage
Real Data	95.90	98.09	93.53	86.24	80.20	72.15	75.68
RandSelect	96.19	98.20	93.85	86.52	80.92	73.35	77.27
SBSim	96.25	98.22	94.04	86.79	80.63	72.16	76.29
Clip-Align	87.21	92.77	83.97	73.26	63.83	54.37	60.87
RealScore	96.25	98.20	93.86	86.47	80.86	73.09	77.04
Ours	96.66	98.45	94.42	87.41	81.50	73.96	77.76

CIFAR-10: We use CIFAR-10-Warehouse [69] as a benchmark, the subset of data in this benchmark is illustrated in Figure 16. The inference results are presented in Table 14.

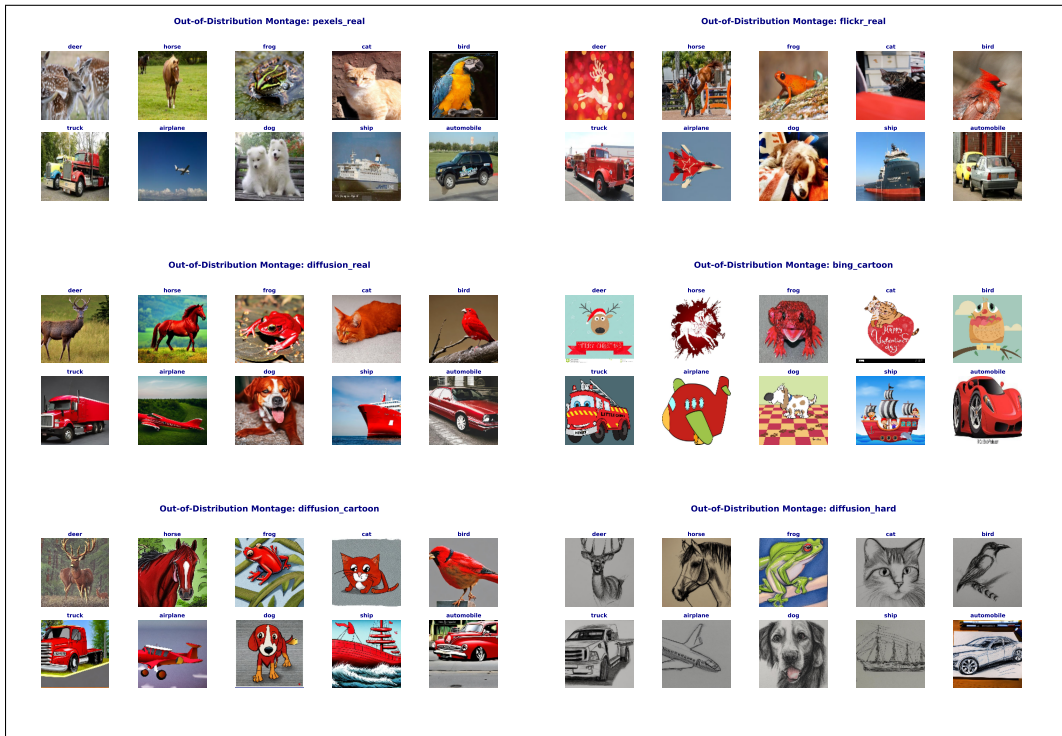


Figure 16: Subsets of CIFAR-10-Warehouse dataset for CIFAR-10 OOD testing.

Table 14: **OOD** Performance comparison on **CIFAR-10**. The best performance for each dataset is highlighted in **bold**.

Method	Diffusion	Flickr	Pexels	360
Original	0.819	0.708	0.810	0.547
Random Sampling	0.904	0.819	0.908	0.655
Similar Only	0.914	0.820	0.908	0.663
CLIP	0.932	0.797	0.898	0.660
Realism	0.924	0.831	0.920	0.679
Ours	0.934	0.850	0.935	0.709

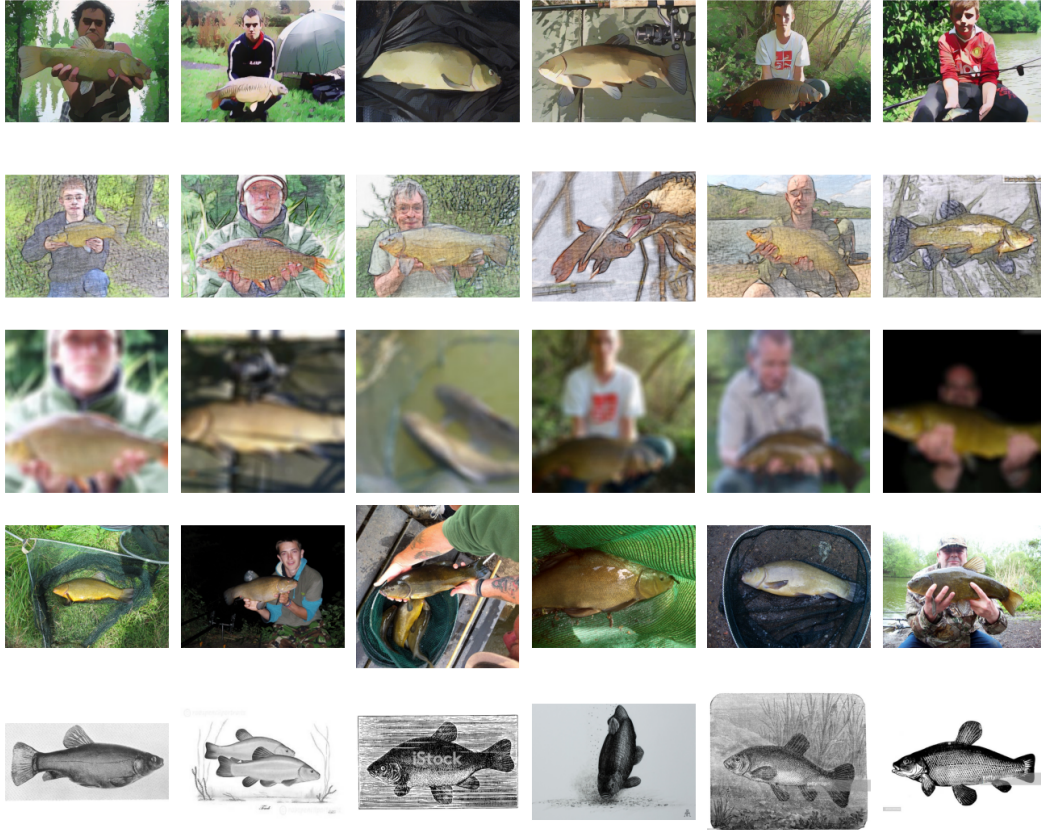


Figure 17: Subsets of IN-1K OOD data

Tiny-ImageNet: We utilize Tiny-ImageNet-C [64] for the evaluation of OOD, which incorporates various types of corruption. We classify them into three types: color-variation set (*i.e.*, brightness adjustment, contrast variation), noise-variation set (*i.e.*, pixelation, Gaussian noise, motion blur), and compression-variation set (*i.e.*, JPEG compression). The results are presented in Table 15.

Table 15: **OOD** Performance comparison on **Tiny-ImageNet**. The best performance for each dataset is highlighted in **bold**.

Method	Color	Noise	Compression
Original	40.52	46.94	48.33
Random Sampling	48.17	46.13	54.23
Similar Only	48.40	53.62	56.89
CLIP	40.52	39.73	40.12
Realism	49.41	52.57	54.23
Ours	52.19	58.77	61.86

ImageNet-1K: We use five ImageNet-1K OOD, illustrated in Figure 17:

- 1) ImageNet-V2 [65] is constructed to closely match the distribution of the original ImageNet-1K, containing 50,000 images across the same 1,000 classes as the original validation set.
- 2) ImageNet-Sketch [66] consists of black-and-white sketches covering all ImageNet-1K classes, with 50 images per class.
- 3) ImageNet-C [67] evaluates model robustness to common corruptions such as noise, blur, weather effects, and digital distortions by applying perturbations with severity levels from 1 to 5 to the original ImageNet validation images.

4) ImageNet-Drawing [68] is derived from the ImageNet validation set, where images are transformed into drawing styles using generative adversarial networks and image processing techniques.

5) ImageNet-Cartoon [68] is also derived from the ImageNet validation set, where images are transformed into cartoon styles.

We categorize them into two main groups based on the sources of image. 1) Original OOD: ImageNet-V2 and ImageNet-Sketch; 2) Derivative OOD: ImageNet-C, ImageNet-Drawing and ImageNet-Cartoon. The inference results is illustrated in the Table 16, 17.

Table 16: **OOD** Performance comparison on **ImageNet-1K** for ViT-B/16. The best performance for each dataset is highlighted in **bold**.

Method	IN-V2-freq.	IN-Sketch	IN-Cartoon	IN-Drawing	IN-C (gaussian)	IN-C (motion)	IN-C (jpeg)	IN-C (snow)
Original	49.86	11.213	43.36	17.494	18.434	30.774	47.668	29.476
Random Sampling	60.57	23.826	58.974	27.728	35.51	41.136	61.364	40.986
SBSim	60.16	23.3	58.554	29.342	33.258	39.736	61.158	39.952
CLIP-Align	56.3	21.193	56.276	32.686	35.086	38.16	58.296	38.08
Realism	60.61	23.73	58.93	27.75	35.48	41.2	61.31	40.88
Ours	61.25	25.308	59.65	30.138	37.226	43.394	62.18	42.666

Table 17: **OOD** Performance comparison on **ImageNet-1K** for ResNet50. The best performance for each dataset is highlighted in **bold**.

Method	IN-V2-freq.	IN-Sketch	IN-Cartoon	IN-Drawing	IN-C (gaussian)	IN-C (motion)	IN-C (jpeg)	IN-C (snow)
Original	56.98	17.34	41.852	14.948	11.418	22.78	41.552	22.46
Random Sampling	60.78	25.29	55.27	26.054	31.518	26.152	53.132	35.906
SBSim	58.81	24.378	52.118	24.762	28.18	25.774	50.156	30.628
CLIP-Align	56.45	24.201	49.996	24.956	27.188	22.928	49.212	27.722
Realism	60.78	25.3	55.25	26.044	31.6	26.13	53.135	35.906
Ours	61.76	26.77	55.404	26.16	35.458	25.93	52.98	34.29

Table 18: Experimental configurations for different datasets, including generator, classifier, and training dataset size.

Dataset	Generator	Synthetic Data Size	Classifier	Training Size
CIFAR-10	EDM	1M	ResNet-18	100K
ImageNet-100	EDM2	1M	ResNet-50	120K

F Additional Analysis

F.1 Limitation of CLIP filter

Reviewing the experimental results, we observe that using CLIP as a filter to select synthetic data consistently leads to the worst performance when training discriminators. Upon inspecting the selected samples, we attribute this degradation to the dominance of monotonous instances. As illustrated in Figure 18, high- and low-CLIP-score examples in Tiny-ImageNet generated by EDM highlight this issue, while Figure 19 presents corresponding cases in ImageNet-1K generated by EDM2. When constructing datasets from a synthetic pool, prioritizing high-CLIP-score instances produces collections enriched with canonical patterns but lacking diversity, ultimately resulting in weaker performance on both in-domain and out-of-domain evaluations.

F.2 Feature Extractor Ablation

Our strategy is built upon image feature representations; therefore, we further investigate whether the choice of feature extractor influences the final performance of classifiers. In this ablation study, we conduct experiments on two datasets: CIFAR-10 and ImageNet-100. The experimental configurations are summarized in Table 18. Specifically, for CIFAR-10, we use EDM to generate 1M synthetic samples and apply our strategy to select 100K training instances, which are then used to train a ResNet-18 model.

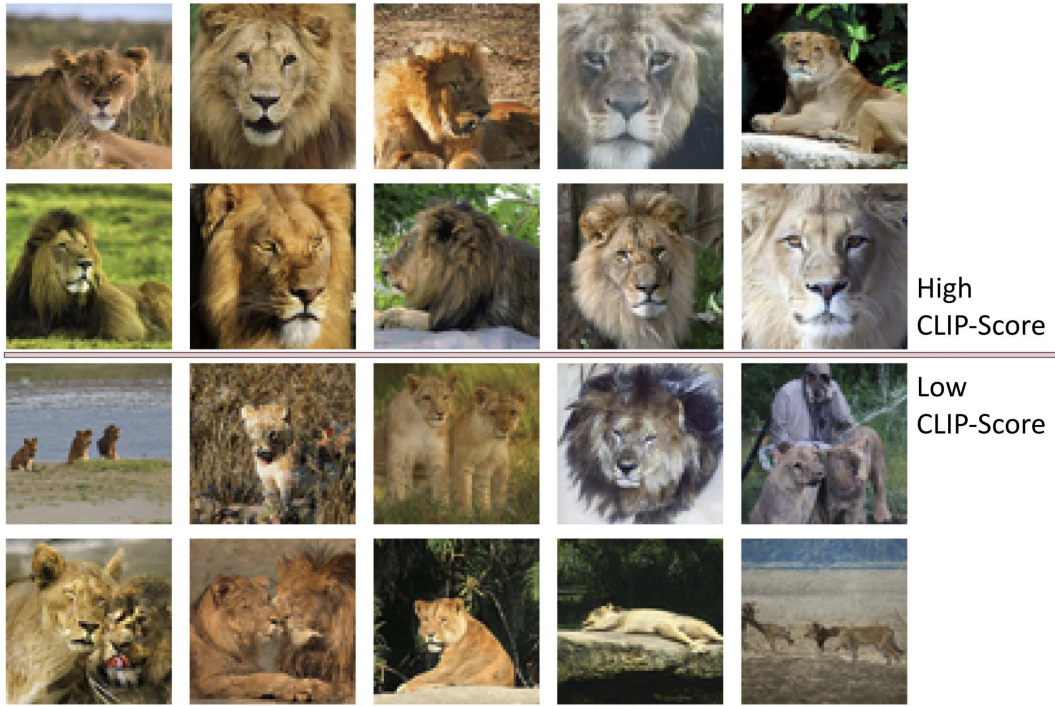


Figure 18: Instances with high and low CLIP-Scores in EDM generated Tiny-ImageNet.



Figure 19: Instances with high and low CLIP-Scores in EDM2 generated ImageNet-1K.

G Implement Details

G.1 Code: scoring

Listing 5: Synthetic alignment scoring

```
def compute_synthetic_common_alignment_scores(
    syn_normed,          # [N, D] normalized synthetic features
    real_common_normed  # [M_1, D] normalized real-common
    synthetic_common_fidelity = syn_normed @ real_common_normed.T

    # diversity score
    centroid_common = F.normalize(real_common_normed.mean(dim=0, keepdim=True), dim=1)
    A = syn_normed.unsqueeze(1) - real_common_normed.unsqueeze(0) # [N, M_1, D]
    B = centroid_common - real_common_normed # [M_1, D]
    numerator = (A * B.unsqueeze(0)).sum(dim=-1) # [N, M_1]
    A_norm = A.norm(dim=-1) # [N, M_1]
    B_norm = B.norm(dim=-1).unsqueeze(0) # [1, M_1]

    synthetic_common_diversity = numerator / (A_norm * B_norm + 1e-8) # [N, M_1]
    synthetic_common_score = synthetic_common_fidelity - synthetic_common_diversity # [N, M_1]
    return synthetic_common_fidelity, synthetic_common_diversity, synthetic_common_score

def compute_synthetic_rare_alignment_scores(
    syn_normed = None, real_rare_normed = None,
    real_np = None, # real features matrix
    class_rare_2_common_in_real_dict = None ):
    synthetic_rare_fidelity = syn_normed @ real_rare_normed.T # [N, M_2]

    rare_2_common_in_real_dict = class_rare_2_common_in_real_dict

    common_counterpart_index = [i["common_image"] for i in rare_2_common_in_real_dict.values()]

    common_counterpart_matrix = get_real_subset_features_matrix(real_np, common_counterpart_index) #
    ↪ [M_2, D]
    normalized_common_counterpart_matrix = F.normalize(common_counterpart_matrix, dim=1) # [M_2, D]

    rare_2_common_matrix = normalized_common_counterpart_matrix - real_rare_normed # shape: [M2, D]
    norm_rare_2_common_matrix = rare_2_common_matrix / rare_2_common_matrix.norm(dim=-1, keepdim=True) #
    ↪ Normalize to unit vectors

    rare_2_synthetic_matrix = syn_normed.unsqueeze(1) - real_rare_normed.unsqueeze(0) # [N, M2, D]
    norm_rare_2_synthetic_matrix = rare_2_synthetic_matrix / rare_2_synthetic_matrix.norm(dim=-1,
    ↪ keepdim=True) # [N, M2, D]

    cos_sim_matrix = (norm_rare_2_synthetic_matrix * norm_rare_2_common_matrix.unsqueeze(0)).sum(dim=-1)
    synthetic_rare_diversity = cos_sim_matrix # [N, M2]
    synthetic_rare_score = synthetic_rare_fidelity - synthetic_rare_diversity # [N, M2]
    return synthetic_rare_fidelity, synthetic_rare_diversity, synthetic_rare_score
```

1 G.2 Code: selection

Listing 6: Top-k synthetic selection

```
def get_the_highest_score_index(matrix, synthetic_name_list, top_k=250, top_n=2, reverse=False):
    if matrix.shape[0] > matrix.shape[1]:
        matrix = matrix.T
        number_of_real = matrix.shape[0]
        number_of_synthetic = matrix.shape[1]
    if reverse:
        matrix = -matrix

    # for each row return the top-n largest column indices and values
    topk_values, topk_indices = torch.topk(matrix, top_n, dim=1) # shape: (rows, top_n)
    # print("the shape of matrix:", matrix.shape)
    assert len(synthetic_name_list) == matrix.shape[1], \
        "Synthetic image names length must match the number of synthetic features."

    retrieval_syn_image_and_scores = {}
    # iterate through each row
    for indices, values in zip(topk_indices, topk_values):
        for idx, val in zip(indices, values):
            current_image_name = synthetic_name_list[idx.item()]
            current_value = retrieval_syn_image_and_scores.get(current_image_name, -9999)
            if val.item() > current_value:
                retrieval_syn_image_and_scores[current_image_name] = val.item()

    # check unique count
    assert len(set(retrieval_syn_image_and_scores.keys())) >= top_k, \
        f"The number of unique top-{top_n} column indices is less than top_k."
    return list(retrieval_syn_image_and_scores.keys()), retrieval_syn_image_and_scores
```

2 H Limitations

3 This work has several limitations, which also point to promising directions for future research.

4 **1) Dependence on generator quality.** Our method operates as a post-generation curation strategy
5 built on top of off-the-shelf generators, without intervening in or steering the generation process itself.
6 As a result, the upper bound of synthetic data utility is inherently constrained by the quality of the
7 generator. When the generator is too weak to produce realistic images, curation may largely reduce
8 to selecting samples with relatively higher fidelity, while diversity-aware selection may become less
9 beneficial because low-fidelity samples can further weaken downstream performance. Nevertheless,
10 as modern generative models continue to improve, synthetic data is becoming increasingly realistic,
11 making post-generation curation more meaningful for unlocking its downstream utility.

12 **2) Limited to unimodal image settings.** Our current method focuses on curating synthetic image
13 data and does not extend to multimodal settings. As vision-language models continue to advance,
14 synthetic datasets that support multimodal training are becoming increasingly important. However,
15 multimodal curation involves data formats beyond images and requires modeling interactions across
16 modalities, which are not addressed by the current framework. Extending post-generation curation to
17 multimodal data is therefore an important and meaningful direction for future work.

18 **3) Reliance on real reference data.** Our method requires a real reference set to construct the
19 $\mathcal{I}_{HO}/\mathcal{I}_{HE}$ partition, which is standard in reference-based curation. In practice, however, only a small
20 reference set is often sufficient, since the partition depends more on relative intra-class similarity than
21 on absolute data scale.

22 **4) Dependence on pretrained feature extractors.** Our scoring procedure relies on pretrained feature
23 extractors. Although Fig. 9 shows that the method is only modestly sensitive to the choice of encoder,
24 a severely domain-mismatched feature extractor may still degrade partition quality. In practice, we
25 recommend using strong general-purpose encoders, such as SigLIP, when domain-specific alternatives
26 are unavailable.

27 I Broader impacts

28 Our work on synthetic data selection raises several ethical considerations that warrant discussion.

29 **Bias Amplification:** Our HOMO-HETERO partitioning strategy could potentially amplify biases
30 present in the original data if the HOMO set disproportionately represents certain demographic groups
31 or patterns. We mitigate this by explicitly incorporating diversity metrics in our selection criteria.

32 **Environmental Impact:** While synthetic data generation incurs computational costs, our selective
33 curation approach reduces the environmental footprint by enabling comparable performance with
34 smaller datasets, requiring fewer training iterations and less storage.

35 **Privacy Preservation:** Although synthetic data generally poses fewer privacy risks than real data, our method does not specifically
36 filter for instances that might inadvertently resemble real individuals. Practitioners should implement
37 additional privacy checks when deploying our method in sensitive domains.

38 **Responsible Use:** We acknowledge that synthetic data technology could be misused for creating deceptive content. Our
39 method is designed for legitimate research and educational purposes, specifically to improve model
40 training efficiency while maintaining performance standards. We encourage adherence to established
41 guidelines for synthetic data use and advocate for continued development of detection methods to
42 distinguish synthetic from real content.